Imperial College London
Department of Physics

Gravitational collapse in asymptotically flat and asymptotically anti-de-sitter spacetime

Miguel Francisco García Vera

September 2012

Supervised by Toby Wiseman Ph.D.

Submitted in part fulfilment of the requirements for the degree of
Master of Science of Imperial College London

Contents

List of Tables

List of Figures

Abstract

We studied the gravitational collapse of the massless scalar field in 3+1 dimensions for asymptotically flat and asymptotically anti-de Sitter (AdS) spacetimes by solving numerically the Einstein-scalar field system of equations. By using double null coordinates we reproduced the results found in the literature for asymptotically flat and asymptotically AdS spacetimes. In both cases we were able to show the existence of the critical solution first discovered by Choptuik in the 1990s. In the case of asymptotically AdS spacetime we studied the solutions for different values of the negative cosmological constant Λ. In addition, given our particular choice for the profile of the initial perturbation, we observe a clear relation between the AdS radius L and the amplitude of the perturbation at the threshold of black hole formation.

1. Introduction

General relativity (GR) is one of the most outstanding scientific breakthroughs of the 20th century. It succesfully explains the properties of the gravitational interaction in the classical regime and provides a model for the general structure of the universe. It also predicted the existence of black holes, which has been later supported by experimental evidence [1]. Moreover, it is widely accepted that our universe began from a space-time singularity, so understanding the limits of the theory in this type of scenarios is of crucial importance to increase our knowledge of the universe.

The basic problem in GR is solving the Einstein Equation for a given energy-matter distribution.

$$G_{\mu\nu} + \Lambda g_{\mu\nu} = 8\pi T_{\mu\nu} \tag{1.1}$$

Where $G_{\mu\nu} = R_{\mu\nu} - \frac{1}{2} g_{\mu\nu} R$ is the Einstein tensor written in terms of the Ricci tensor $R_{\mu\nu}$ and the Ricci scalar R. $T_{\mu\nu}$ is the stress energy tensor related to the matter content of spacetime. The constant Λ is the cosmological constant.

The Einstein field equations give rise to a non-linear system of differential equations which usually can not be solved analytically. Therefore, there is a great effort put into developing numerical techniques to solve this type of problems for different spacetime models, and particularly for the case where black holes appear.

For long time it was known that strong enough initial configurations of matter would lead to black hole formation, while weak enough initial configurations are dispersed to infinity. However, little was known of the intermediate scenario in the threshold of black hole formation. One remarkable result was obtained by Choptuik [2] for the collapse of the massless scalar field in spherical symmetry. Choptuik showed that by choosing an specific initial configuration, the evolution of the spacetime approaches a unique scale-invariant solution with a massless central singularity.

The type of behaviour observed by Choptuik is similar to the critical phenomena

observed in phase transitions in statistichal mechanics. In both cases, critical phenomena is characterized by fine-tuning, universality, scale-invariant physics, and critical exponents for dimensionful quantities. Some examples include the liquid-gas phase transition or the magnetisation in ferromagnetic materials. In the case of ferromagnetic materials, one is interested in the magnetisation m as a function of temperature T. The system shows a well known behaviour for temperatures close to the Curie temperature T^* characterized by:

$$m \propto (T^* - T)^\gamma \tag{1.2}$$

Where γ is a critical parameter associated with the phase transition and m is known as the order parameter. Situations where the order parameter changes discontinuously at the transition are known as Type I phase transtions, whereas situations where the order parameter goes to zero continuously are known as Type II phase transitions. Interestingly, the case of gravitational collapse behaves in the same way with the black hole mass M acting as the order parameter. Moreover, by fine-tuning the initial data, one finds a self-similar solution ϕ^* characterized by its dimensionless period Δ, such that:

$$\phi^*(r,t) = \phi^*(e^{n\Delta}r, e^{n\Delta}t) \tag{1.3}$$

The discovery of Choptuik raised questions regarding whether the critical phenomena is a general feature of gravitational collapse or only a particular result for the spherically symmetric case that he studied. In the following years, several authors have found that this kind of phenomena is not restricted to the case studied by Choptuik, and therefore, critical phenomena is a general feature of gravitational collapse.

Clearly, the study of gravitational collapse has great relevance in the fields of astrophysics and cosmology. Most of the work in the subject is concerned with assymptotically flat spacetimes. Only recently, the study of asymptotically anti de-Sitter (AAdS) spacetimes has become of greater interest, mainly due to the ADS/CFT conjecture [3], also known as gauge/gravity duality. This conjecture states that there is an equivalence between two theories. One of them is a gravity theory on a d+1 dimensional spacetime with a d dimensional asymptotic boundary, and the other is a d dimensional quantum field theory living in its boundary. The simplest and most studied scenario is the one in which the gravity theory is defined in an AAdS spacetime, and it is related to a conformal field theory on its boundary. The applications of this equivalence are now on the frontier of experimental and theoretical research.

From that perspective, it is desirable to understand the problem of gravitational collapse in AAdS spacetimes. Perhaps one of the most important results in that respect can be attributed to the recent work of Bizon and Rostworowski [4] showing that unlike assymptotically flat spacetimes, AAdS spacetimes are not stable under arbitrarily small perturbations and there is no a definitive threshold for black hole formation, unlike the case of asymptotically flat spacetime. In spite of that, the qualitative behaviour of the gravitational collapse in AdS is similar to the one observed in the flat case. In both cases, the gravitational collapse is characterized by the presence of the critical behaviour found by Choptuik.

In this thesis we will focus on the study of the critical parameters γ and Δ of the critical solution in asymptotically flat and AAdS spacetimes in 3+1 dimensions. In section 2 we make a brief review of critical phenomena in gravitational collapse. In section 3 we introduce the mathematical formalism to solve the Einstein equations in both assymptotically flat and AAdS spacetimes. In section 4 we describe the numerical methods used to solve the set of differential equations and in section 5 we present our results. We considered a 1-parameter family of initial data characterized by a parameter A, which was fine-tuned to A^* at the threshold of black hole formation. Our choice of double null coordinates has been proven to work in asymptotically flat spacetime, but it is a new result in the case of asymptotically AdS_4 spacetimes. Our results reproduce up to computational resources the results found by Hamade and Stewart [5] and originally by Choptuik [2] for the massless scalar field in asymptotically flat spacetime. In the case of AAdS, we have found the same critical parameters as for the asymptotically flat case, in accordance with the results reported in the literature [4]. Additionally, given our particular choice for the initial perturbation, we show the existence of a relation between the parameter A^* at the critical solution, and the AdS radius L. We observe that A^* asymptotes rapidly towards its value in asymptotically flat spacetime.

2. Gravitational Collapse and Critical Phenomena

2.1. Asymptotically flat spacetime

The study of gravitational collapse in asymptotically flat spacetime has great relevance for its implications in astrophysics, cosmic censorship and quantum gravity. Particularly, the pioneer work of Choptuik on the gravitational collapse of the massless scalar field in spherical symmetry [2] showed some interesting phenomena associated with solutions close to the threshold of black hole formation. The results of Choptuik can be summarized as:

1. Black hole mass scaling: $M = k(p - p^*)^\gamma$
2. Universality of the critical solution
3. Scale echoing of the critical solution

The parameter p parametrizes a particular one-paramter family of initial data. The constant k and the critical value p^* depend on the particular one-parameter family, while the exponent γ is universal. The critical value p^* is such that for $p > p^*$ the evolution of the original perturbation leads to collapse and black hole formation, while for $p < p^*$, the perturbation is dispersed to infinity. Interestingly, near p^* the evolution approaches a universal solution independent of the initial shape of matter distribution, which is called the critical solution. The third property implies that the critical solution is scale invariant by a factor of e^Δ, where Δ is a universal echoing period independent of the initial data.

$$\phi^*(r, t) = \phi^*(e^\Delta r, e^\Delta t). \tag{2.1}$$

The existence of the critical solution found by Choptuik has some important consequences as it suggests that regions of arbitrarily large curvature could be achieved outside a black hole. Hence, in the limit of perfectly well tuned initial data, naked singularities

could appear, in contradiction to the cosmic censorship conjecture. This suggestion has been further studied under different conditions, not restricting it to the spherically symmetric case [6, 7, 8, 9, 10]. However, these results are not generic enough to impose a contradiction to the cosmic censorship conjecture, and it remains an open question.

Following Choptuik's work, many different models have been studied, including scalar fields in 2+1, 4+1 and higher spacetime dimensions [11], vector and spinor fields [12], perfect fluid matter [13, 14], collisionless matter [15, 16], sigma models [17, 18], Yang-Mills fields [19], and others. For a complete review, see [20]. In all cases, critical phenomena similar to the one observed by Choptuik was found. The general characteristics of the criticality can be summarized as:

1. Δ and γ are universal for a given model, independent of the one parameter family of initial data.

2. There are two types of critical phenomena, which are related to the symmetry properties of the critical solution. The critical phenomena found by Choptuik corresponds to type II, where the critical solution is scale invariant (either showing continuous self similarity (CSS) or discrete self similarity (DSS)) and the order parameter M is continuously turned on at the critical value p^*. Type I critical phenomena shows stationary or time periodic critical solution and the order parameter M is finite when a black hole is formed.

It is interesting that such critical solutions in GR correspond to spacetimes with extra spacetime symmetries unlike a regular solution in the phase space. Some of the models can also show a mixed type of symmetry, as for example transition between DSS and CSS [21], or a mix of type I and type II critical phenomena in different regions [22].

The critical phenomena can be explained by considering GR as an infinite dimensional continuous dynamical system. The points in the phase space are sets of 3 metrics and extrinsic curvatures plus any matter variable that obey the Hamiltonian and momentum constraints. The phase space has (at least) two attacting fixed points which correspond to dispersion or black hole formation. The boundary between the two basins of attraction is the critical surface which has one attracting point itself which is the critical solution found by Choptuik. Figure 2.1 illustrates the origin of universality. Basically, any initial data that is close to the threshold of black hole formation approaches the critical solution in a trajectory that is tangential to the critical surface. Finally, when it approaches the critical solution, it either disperses or collapses into a black hole following a trajectory which seems to originate in the critical solution, therefore the information of the initial configuration has been forgotten, except for the distance to the critical surface.

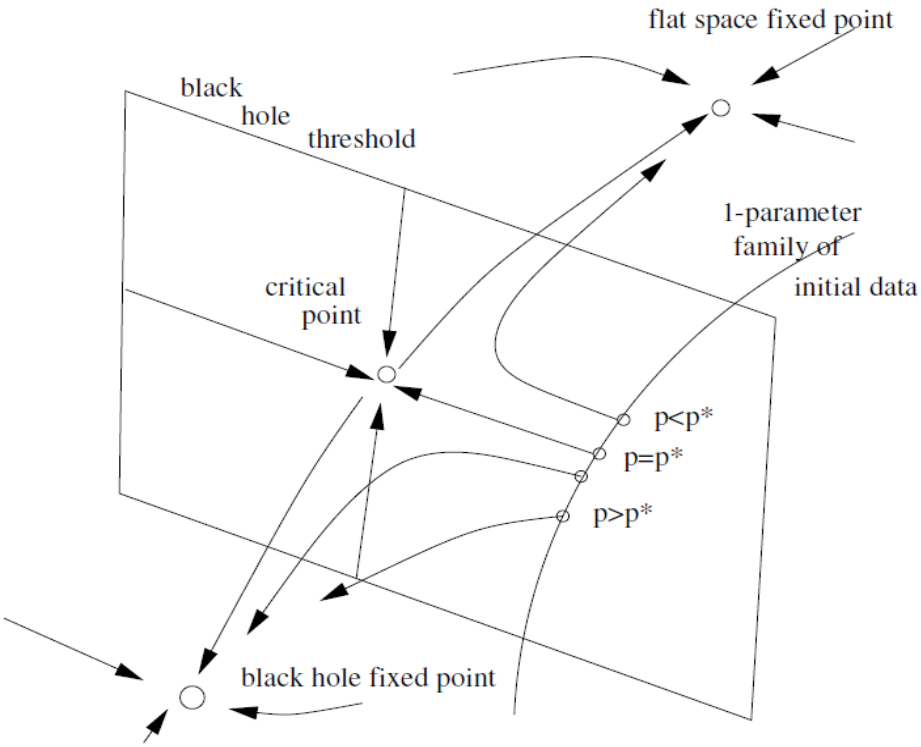

Figure 2.1.: Phase space diagram of gravitational collapse. The arrow lines represent the evolution of spacetime solutions. The arrowless line corresponds to a 1-parameter family of initial data. Subcritical data $p < p^*$ approaches the critical solution and then deviates towards the flat space fixed point, while supercritical data $p > p^*$ deviates toward the black hole fixed point [20].

The critical solution acts as a codimension one attractor in the phase space, which means that it has only one growing mode not tangential to the critical solution characterized by its eigenvalue λ. This fact has been verified by constructing the critical solution explicitly. To do that, one has to solve the relevant PDE system with the assumptions of spherical symmetry, discrete self-similarity (DSS) and analyticity at the past center and past light cone of the singularity [24]. Discrete self-similarity is formally introduced by considering there exists a diffeomorphism Φ and a constant Δ, such that for any integer n:

$$(\Phi_*)^n \, g_{\mu\nu} = e^{2n\Delta} g_{\mu\nu} \tag{2.2}$$

Where Φ_* is the pullback of Φ.

One can then introduce coordinates (σ, x^μ) such that if p has coordinates (σ, x^μ), then $\Phi(p)$ has coordinates $(\sigma + \Delta, x^\mu)$. In these coordinates, DSS is expressed as:

$$g_{\mu\nu}(\sigma, x^\alpha) = e^{2\sigma} \hat{g}_{\mu\nu}(\sigma, x^\alpha) \tag{2.3}$$

Where, $\hat{g}_{\mu\nu}(\sigma, x^\alpha) = \hat{g}_{\mu\nu}(\sigma + \Delta, x^\alpha)$.

Gundlach constructed the solution for the massless scalar field in a spherically symmetric background asuming equation 2.3 is satisfied [17]. To do that, he chose coordinates τ and ζ which satisfy the conditions stated previously:

$$\tau = \ln\left(\frac{t}{r_0}\right), \qquad \zeta = \ln\left(\frac{r}{t}\right) - \eta_0(\tau) \tag{2.4}$$

Where r_0 is a fixed scale and $\eta_0(\tau)$ is a periodic function in τ with a period Δ. r and t are the regular variables in spherical coordinates. Gundlach solved the Einstein-scalar system and found $\Delta = 3.4454 \pm 0.0005$, which is in agreement with the value obtained by Choptuik.

This description of gravitational collapse has been used to explain the origin of the mass scaling law by using linear perturbation analysis and more generally by using renormalization group flow techniques [23]. Briefly, we consider a general spherically symmetric line element of the form:

$$ds^2 = -\alpha^2 dt^2 + f^{-1} dr^2 + r^2 d\Omega^2 \tag{2.5}$$

A perturbation of the metric parameter f of the self-similar critical solution can be written as [25]:

$$\pm |p - p^*| f_1(x) t^{-\lambda} \tag{2.6}$$

Where $x = r/t$ and the $\pm$ corresponds to dispersion or black hole formation. An apparent horizon at (x_H, t_H) is characterized by $f(x_H, t_H) = 0$ so that:

$$f^*(x_H) \pm |p - p^*| f_1(x_H) t_H^{-\lambda} = 0 \tag{2.7}$$

The black hole mass M at the apparent horizon is equal to $r_H/2$, so by substituting $t_H = r_H/x_H$ in equation 2.7 and solving for r_H we obtain:

$$M = r_H/2 \propto |p - p^*|^{1/\lambda} \tag{2.8}$$

Where the scaling exponent γ found by Choptuik is related to the eigenvalue of the growing perturbation as:

$$\gamma = 1/\lambda \tag{2.9}$$

Gundlach considered the linear perturbations of the critical solution which leave the perturbed solution regular at $r = 0$ and $\zeta = 0$. In his work, he found $\gamma = 0.374 \pm 0.001$ [17], in agreement with the value reported by Choptuik [2] and more accurately by Hamade and Stewart [5] in the simulations of gravitational collapse.

Similar scaling laws have been found for the charge in massless scalar electrodynamics [26, 27], with a critical exponent δ satisfying the inequality $\delta \geq 2\gamma$.

It must be mentioned that the study of gravitational collapse in asymptotically flat spacetime is far from being complete. In particular, there is a great interest in numerical scenarios which do not show spherical symmetry. Some attempts to go beyond spherical symmetry have considered small perturbations of the spherically symmetric case, and the authors in [8] have shown that the only growing mode corresponds to the spherical mode with $\lambda = 2.7$, but they conjecture that the relatively small decay rate for the least damped mode $\lambda = -0.2$ could be observed for an intermediate range of $p - p^*$.

Even further beyond spherical symmetry, there are promissing results when considering axisymmetry. Choptuik, Hirschmann, Liebling and Pretorius have studied the numerical evolution for a axisymmetric massless scalar field, and the critical behaviour has also been observed [28, 29]. In their simulations, they have found an extra unstable mode besides the spherical one, which is responsible for an splitting in the critical solution.

2.2. Asymptotically AdS spacetime

The case of gravitational collapse in AAdS spacetime has been studied in much less depth than the asymptotically flat case. Recently it has become of greater interest due to the AdS/CFT conjecture. In particular, this relation makes it possible to obtain predictions for QFT theories at strong coupling by solving the dual gravitational problem in the bulk.

Among others, this approach has been used to understand phenomena such as properties of superconductors [30], non-Fermi liquid systems [31] and the thermalization and evolution of strongly coupled plasma [32, 33]. In all these models the formation of a black hole plays a key role on describing the thermodynamical properties of the system.

The case of thermalization and evolution of strongly coupled plasma has particularly been studied by modelling the gravitational collapse in AdS_5 spacetime [34, 35]. In this case, the evolution of spacetimes with black hole formation is equivalent to non equilibrium dynamics and thermalization in field theory, where the thermalization of the strongly coupled plasma corresponds to the formation of a black hole in the bulk. As has been pointed out in [35], the gauge/gravity duality is of great pratical interest to understand the results of the RHIC and LHC (ALICE) experiments. In [35] the authors proposed an intimate relation between the time of apparent horizon formation and quantities which depend on the thermalization time.

The most important feature of AdS which differentiates it from flat or de-sitter spacetimes is the fact that it has a timelike boundary at space and null infinity. Therefore, the Cauchy problem is not properly defined unless appropiate boundary conditions are imposed (see Appendix A). A perturbation which is initially ingoing will interfere in the origin and become outgoing towards future null infinity. Once it reaches infinity, it will be reflected and will eventually return to the origin in a finite proper time. In figure 2.2 we show the conformal diagram of AdS before compactification of the time coordinate. A radial null geodesic will be reflected an infinite number of times from the time-like boundary at null infinity (see Appendix A for an explanation of the coordinates).

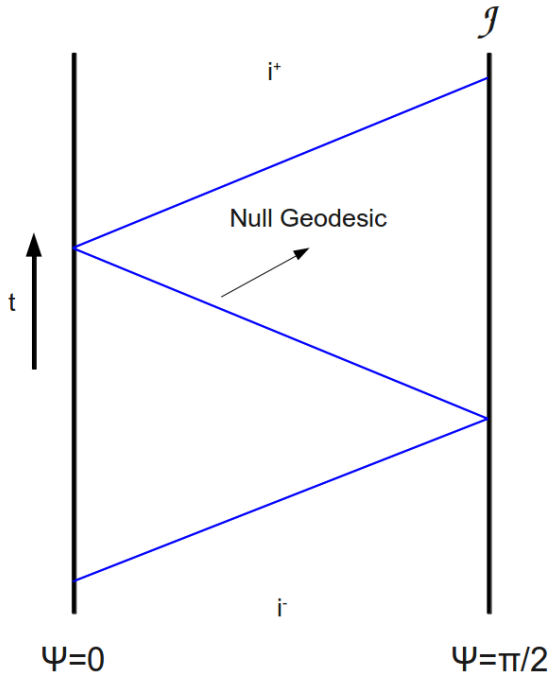

Figure 2.2.: Conformal diagram of AdS spacetime. The conformal boundary at null infinity ($\mathcal{J}$) looks like an infinitely long time-like line, so a null geodesic will bounce indefinitely many times on the boundary at null infinity. Past and future time-like infinity are depicted as the points i^- and i^+ and are not included in the boundary because we have not considered the compactification in the time direction.

The existence of the time-like boundary at future null infinity is of particular importance to the numerical simulations because one has to limit the evolution to a finite number of reflections. Considering this fact, some authors have studied the case of black hole formation before the first reflection and have found a critical behaviour just as the one observed in the flat case [36, 37, 38]. Basically, the evolution approaches a universal solution which exhibits self-similar behaviour as the type II critical phenomena observed in the gravitational collapse in asymptotically flat spacetime. Type I critical phenomena is expected to appear under certain circumstances but it is still an open question regarding collapse in AAdS.

The boundary problem in AdS is particularly important when considering the stability of AAdS spacetimes. Recently, Bizon and Rostorowski [4] studied the gravitational collapse of a real massless scalar field on 3+1 and 4+1 dimensions using non-flux boundary conditions and found that unlike the asymptotically flat case, the evolution of the original perturbation inevitably leads to black hole formation. Their explanation is more general as they provide a theoretical framework to explain the character of the instability. By considering a weakly perturbed solution of the Einstein equations, the authors showed that the solution tends to shift their energy from lower to higher frequencies which inevitably leads to concentration of energy in smaller scales and consequently the formation of black holes.

To notice the origin of the instability, Bizon and Rostorowski use a coordinate system in which the metric for an asymptotically AdS_{d+1} spacetime is written as:

$$ds^2 = \frac{L^2}{\cos^2(x)}\left(-A(t,x)e^{-2\delta(t,x)}dt^2 + A^{-1}(t,x)dx^2 + \sin^2(x)d\Omega_{d-1}^2\right) \tag{2.10}$$

Where $L^2 = -d(d-1)/2\Lambda$ is the AdS radius (see Appendix A) and $d\Omega_{d-1}^2$ is the metric on S^{d-1}. The coordinates take the values of $-\infty < t < \infty$ and $0 \leq x \leq \pi/2$. In this metric, the evolution of the linear perturbations in AdS_{d+1} is determined by the self adjoint operator $\hat{L} = -\tan^{1-d} x\partial_x \left(\tan^{d-1} x\partial_x\right)$, whose spectrum is given by $w^j = (d+2j)^2$, $(j = 0, 1, \ldots)$. The authors then show that one gets resonant terms within third order nonlinear perturbation analysis. The resonance appears in the mode w^j such that $j = j_1 + j_2 - j_3$, where j_k are the indices for the eigenmodes present in the original perturbation.

The instability is shown by following the evolution of a 1-parameter family of initial data. By choosing strong enough initial data, the solution would collapse before any reflection in the AdS boundary, and locally the solution approaches the one found by

Choptuik for the case $\Lambda = 0$. By decreasing the amplitude of the pulse, the perturbation is reflected in the AdS boundary and collapses again. This pattern was confirmed for up to 10 reflections, and in every case, the solution approaches the Choptuik solution. One should imagine the perturbation travelling through the path of the null geodesic in figure 2.2, which will bounce at $\mathcal{J}$ as the time of the simulation increases.

The question of linear stability on AAdS spacetimes is still an open area of research. In that context, the role of the cosmological constant is key in the causal properties of AdS, and as such, there are a lot of questions regarding its role in the black hole formation in AAdS. Particularly, it is still unknown whether the cosmological constant, which acts as an extra attractive force in the Einstein equations triggers the black hole formation for arbitrarily small perturbations, or maybe its only role is the confinement of the evolution within a time-like bound surface. This type of questions are raised by the authors of [4]. Additionally, a negative cosmological constant is required for black hole solutions in 2+1 dimensions [39]. No black holes are formed in the case where the cosmological constant is equal to zero. The black hole solutions in 2+1 dimensions are known as BTZ black holes and exhibit properties very similar to the ones observed in their traditional 3+1 counterparts.

3. Einstein Scalar Equations

The structure of spacetime is basically determined by the form of the metric g in equation 1.1. By solving the Einstein equations we aim at defining the metric components $g_{\mu\nu}$ for a given matter field and for a given value of the cosmological constant Λ.

The Einstein equations can be obtained by a variational principle by introducing the Einstein-Hilbert action S:

$$S = \int \left[\frac{1}{16\pi} (R - 2\Lambda) + \mathcal{L}_M \right] \sqrt{-g} \, \mathrm{d}^4 x \tag{3.1}$$

Where $\mathcal{L}_M$ is the Lagrangian density for the matter fields considered. The stress-energy tensor is then defined by:

$$T_{\mu\nu} = \frac{-2}{\sqrt{-g}} \frac{\delta \left(\sqrt{-g} \mathcal{L}_M \right)}{\delta g^{\mu\nu}} \tag{3.2}$$

Given that both sides in equation 1.1 are symmetric, there will be ten coupled non-linear partial differential equations for the metric and its first and second derivatives in a 3+1 dimensional space.

By adding the conservation equation:

$$T^{\mu\nu}{}_{;\nu} = 0 \tag{3.3}$$

We end up with a system of 6 non-linear partial differential equations to solve.

An important feature of GR is the fact that the gravitational field is self-interacting. The equations are non-linear in the absense of other fields or any material sources. Additionally, unlike Maxwell theory for example, the solutions for the Einstein equations are not to be found for a fixed background; on the contrary, the space-time manifold itself is part of the solution.

The numerical approach to solve the Einstein equations is then expressed in terms of the Cauchy problem for a system of non-linear differential equations. The Cauchy problem consists in establishing a correspondence between the solution and the data given in a suitable initial hypersurface. For the case of linear hyperbolic equations there is always possible to find such solution, however, in the case of GR we are dealing with a non-linear system and the Cauchy problem is not always satisfied in the broader sense (See appendix A for the particular case of AdS spacetime).

We can re-write equation 1.1 in the form:

$$R_{\mu\nu} - \Lambda g_{\mu\nu} = 8\pi \left(T_{\mu\nu} - \frac{1}{2} T g_{\mu\nu} \right) \tag{3.4}$$

So that the higher order components of the differential operator that acts on g are given by:

$$R_{\mu\nu} = -\frac{1}{2} g^{\lambda\rho} \left(\frac{\partial^2 g_{\mu\nu}}{\partial x^\lambda \partial x^\rho} + \frac{\partial^2 g_{\lambda\rho}}{\partial x^\mu \partial x^\nu} - \frac{\partial^2 g_{\mu\rho}}{\partial x^\lambda \partial x^\nu} - \frac{\partial^2 g_{\rho\nu}}{\partial x^\mu \partial x^\lambda} \right) + Q_{\mu\nu}\left(g, \partial g\right) \tag{3.5}$$

Where Q is a rational function of the metric and its first derivatives. We can see that the system of equations is at most quasi-linear. The authors in [40] make a complete review on the Cauchy problem for the general d-dimensional Einstein equations taking into consideration the quasi-linearity of the field equations.

3.1. Arnowitt-Deser-Misner (ADM) formalism

To treat the Cauchy problem in GR, most approaches are based on the Arnowitt-Deser-Misner (ADM) formalism, so for completeness we briefly discuss its main results in the following.

The Cauchy problem can be formulated by defining an initial hypersurface S with intrinsic metric components h_{ab} $(a, b = 1, 2, 3)$, on which the initial conditions are imposed. Then, the metric can be written in the ADM representation, where we define t in such a way that the vector field T given by $T = \partial_t$ is transverse to the hypersurface S:

$$g = -\alpha^2 dt^2 + h_{ab} \left(\beta^a dt + dx^a \right) \left(\beta^b dt + dx^b \right) \tag{3.6}$$

Where α is the lapse function and $\beta = \beta^a \partial_a$ is the shift vector field.

Next we define a unit normalized vector, n^μ:

$$n^\mu = -\alpha g^{\mu\nu} \nabla_\nu t \tag{3.7}$$

Which is a time-like future pointing unit vector normal to the hypersurface S. We can now construct the projection operator $\gamma^\mu_\nu = \delta^\mu_\nu + n^\mu n_\nu$ which allows us to define the extrinsic curvature $\chi_{\mu\nu}$ as the projection of the gradient of the normal vector on S:

$$\chi_{\mu\nu} = -\gamma^\lambda_\mu \gamma^\rho_\nu \nabla_\lambda n_\rho = -D_\mu n_\nu \tag{3.8}$$

Where $D_\mu = \gamma^\nu_\mu \nabla_\nu$ is the projection of the covariant derivative in S. Equivalently, χ can be related to the Lie derivative of the intrinsic metric h by:

$$\mathcal{L}_T h_{\mu\nu} = 2\alpha \chi_{\mu\nu} + \mathcal{L}_\beta h_{\mu\nu} \tag{3.9}$$

The extrinsic curvature and the intrinsic metric define the state of the gravitational field as a dynamical system. In the ADM formalism, the Einstein equations are then split into constraint equations which must be fulfilled at every time slice hypersurface $t = constant$, and evolution equations which evolve χ and h from one slice to the next. The constraint equations are obtained by fully contracting the Einstein equation with n^μ twice and by contracting with n^μ once and then projecting onto S:

$$n^\mu n^\nu \left(G_{\mu\nu} + \Lambda g_{\mu\nu} - 8\pi T_{\mu\nu} \right) = 0 \tag{3.10}$$

$$n^\mu \gamma^\rho_\nu \left(G_{\mu\rho} + \Lambda g_{\mu\rho} - 8\pi T_{\mu\rho} \right) = 0 \tag{3.11}$$

Which leads to:

$${}^3R - \chi_{ab}\chi^{ab} + \chi^2 - 2\Lambda - 16\pi\rho = 0 \tag{3.12}$$

$$D_a \chi^a_b - D_b \chi^a_a + 8\pi j_b = 0 \tag{3.13}$$

Where ${}^3R$ denotes the Ricci scalar on S, $\rho = n^\mu n^\nu T_{\mu\nu}$ and $j_\nu = -n^\mu \gamma^\rho_\nu T_{\mu\rho}$. The two

equations are known as the Hamiltonian and Momentum constraints respectively.

The evolution equations are obtained by fully projecting the Einstein equation on S:

$$\gamma_{\mu}^{\lambda}\gamma_{\nu}^{\rho}\left(G_{\lambda\rho}+\Lambda g_{\lambda\rho}-8\pi T_{\lambda\rho}\right)=0 \tag{3.14}$$

Which leads to the equation:

$$\partial_t\chi_{ab}=-\alpha\left({}^3R_{ab}+\chi_c^c\chi_{ab}-2\chi_{ac}\chi_b^c\right)+D_aD_b\alpha+\mathcal{L}_\beta\chi_{ab}+\alpha\left(\Lambda h_{ab}+8\pi\left(T_{ab}-\frac{1}{2}Th_{ab}\right)\right) \tag{3.15}$$

Where $\mathcal{L}_\beta$ is the Lie derivative with respect to the vector field β. Equations 3.15 and 3.9 define the evolution from one slice to the next.

The ADM formalism is defined by considering a spacelike initial hypersurface. However, the results are general regardless of the initial Cauchy surface. In general, for the numerical resolution of the Einstein equations one defines an initial Cauchy surface and imposes the initial conditions which satisfy the constraint equations. The procedure then evolves all the variables slice by slice to cover the submanifold that is being considered.

3.2. Null coordinates

In GR one has the freedom to choose a convenient set of coordinates depending on the symmetry of the problem. In particular one can choose coordinates u, v in which ingoing/outgoing radial null geodesics are given by $u/v = constant$. Such coordinates are called null coordinates, or double null coordinates. This type of coordinates are particularly useful when one wants to study the causal properties of a system, due to the simple representation of light-like geodesics.

3.2.1. Minkowski spacetime and Schwarzschild black hole

The line element for Minkowski spacetime is given by:

$$ds^2=-dt^2+dx^2+dy^2+dz^2=-dt^2+dr^2+r^2d\Omega^2 \tag{3.16}$$

In this case, the definition of null coordinates is straightforward. By choosing $u = t - r$ and $v = t + r$ the metric takes the form:

$$ds^2 = -dudv + r^2(u, v)d\Omega^2 \tag{3.17}$$

With $r(u, v) = (v - u)/2$.

Clearly, ingoing/outgoing radial null geodesics are given by $u/v = constant$.

The Schwarzschild black hole metric in its standard form is given by:

$$ds^2 = -\left(1 - \frac{2M}{r}\right)dt^2 + \left(1 - \frac{2M}{r}\right)^{-1} dr^2 + r^2 d\Omega^2 \tag{3.18}$$

In order to define the null coordinates in this case we first make a change of variables in such way that:

$$\frac{dr^*}{dr} = \left(1 - \frac{2M}{r}\right)^{-1} \tag{3.19}$$

Where r^* is known as the tortoise coordinate. Then, the ingoing and outgoing radial null coordinates can be defined as $u = t - r^*$ and $v = t + r^*$. With this choice, the line element takes the form:

$$ds^2 = -\left(1 - \frac{2M}{r(u, v)}\right)dudv + r(u, v)^2 d\Omega^2 \tag{3.20}$$

Where r is determined by the relation:

$$\frac{1}{2}(v - u) = r^* = r + 2M \ln(r - 2M) \tag{3.21}$$

We can observe that this expression of the metric in double null coordinates is conformally flat when $\Omega = constant$.

3.2.2. AdS spacetime and AdS Schwarzschild black hole

Here we begin directly from the standard form of the AdS line element. See Appendix A for details.

$$ds^2 = -\left(1 + \frac{r^2}{L^2}\right) dt^2 + \left(1 + \frac{r^2}{L^2}\right)^{-1} dr^2 + r^2 d\Omega^2 \tag{3.22}$$

Where $L^2 = -3/\Lambda$. As we did in the case of the Schwarzschild black hole, we can make a change of coordinates such that:

$$\frac{dr^*}{dr} = \left(1 + \frac{r^2}{L^2}\right)^{-1} \tag{3.23}$$

And then define the ingoing and outgoing null coordinates as $u = t - r*$ and $v = t + r*$. The metric then can be written as:

$$ds^2 = -\left(1 + \frac{r(u,v)^2}{L^2}\right) dudv + r(u,v)^2 d\Omega^2 \tag{3.24}$$

And by considering the explicit form of r:

$$r = L \tan\left(\frac{r^*}{L}\right) = L \tan\left(\frac{v-u}{2L}\right) \tag{3.25}$$

The metric takes the final form:

$$ds^2 = -\sec^2\left(\frac{v-u}{2L}\right) dudv + L^2 \tan^2\left(\frac{v-u}{2L}\right) d\Omega^2 \tag{3.26}$$

For the case of the Schwarzschild black hole in AdS_4 we have the standard form of the metric [41]:

$$ds^2 = -\left(1 + \frac{r^2}{L^2} - \frac{2M}{r}\right) dt^2 + \left(1 + \frac{r^2}{L^2} - \frac{2M}{r}\right)^{-1} dr^2 + r^2 d\Omega^2 \tag{3.27}$$

And following the same procedure explained previously we define a new coordinate r^* by:

$$\frac{dr^*}{dr} = \left(1 + \frac{r^2}{L^2} - \frac{2M}{r}\right)^{-1} \tag{3.28}$$

And the usual ingoing and outgoing null coordinates u and v, so that the metric takes the form:

$$ds^2 = \left(1 + \frac{r(u,v)^2}{L^2} - \frac{2M}{r(u,v)}\right) dudv + r(u,v)^2 d\Omega^2 \tag{3.29}$$

Where the expresion for $r(u,v)$ is given implicity by the relation in equation 3.28 and the definitions of u and v.

3.3. Einstein Scalar equations for the massless scalar field

In this work we study the gravitational collapse of the spherically symmetric massless scalar field in a 3+1 Minkowski and AdS background. In both cases we are interested in solving numerically the Einstein equations for different initial conditions and study the criticality at the threshold of black hole formation.

Our goal is to solve numerically the Einstein-scalar system governed by the Einstein equations:

$$R_{\mu\nu} - \frac{1}{2}Rg_{\mu\nu} + \Lambda g_{\mu\nu} = 8\pi\left(\Phi_{,\mu}\Phi_{,\nu} - \frac{1}{2}g_{\mu\nu}g^{\alpha\beta}\Phi_{,\alpha}\Phi_{,\beta}\right) \tag{3.30}$$

And the wave equation:

$$\Box_g \Phi = 0 \tag{3.31}$$

Where $\Box_g$ is the D'Alembertian operator with respect to the metric g.

Due to the particular form of the stress energy tensor, in this case it is more convenient to use equation 3.4 so that the system reduces to the form:

$$R_{\mu\nu} - \Lambda g_{\mu\nu} = 8\pi\Phi_{,\mu}\Phi_{,\nu} \tag{3.32}$$

First, we describe the equations in the case where $\Lambda = 0$ and later we modify our

equations to solve the case when $\Lambda < 0$.

We decided to use null coordinates as they are a natural choice which explicitly show the causal structure of spacetime and the metric does not break down at the formation of an apparent horizon. Moreover, previous works using this type of coordinates have shown numerical stability for near critical solutions [5, 38].

We choose to define the general line element in null coordinates as in [5], which is consistent with equations 3.17 and 3.20. The line element is then written as:

$$ds^2 = -a^2(u,v)dudv + r^2(u,v)d\Omega^2 \tag{3.33}$$

3.3.1. $\Lambda = 0$

The wave equation 3.31 can be written in a convenient way as:

$$\partial_\nu \left(\sqrt{-g} g^{\mu\nu} \partial_\mu \Phi\right) = 0 \tag{3.34}$$

From now on we will use the usual convention to denote partial derivatives as $\frac{\partial F}{\partial u} = F_u$, and by considering a spherically symmetric spacetime the wave equation reduces to the form:

$$r\Phi_{uv} + r_u\Phi_v + r_v\Phi_u = 0 \tag{3.35}$$

With our parametrization of the metric we obtain for the relevant components of the Ricci tensor:

$$R_{uu} = \frac{4a_u r_u}{ar} - \frac{2r_{uu}}{r} \tag{3.36}$$

$$R_{vv} = \frac{4a_v r_v}{ar} - \frac{2r_{vv}}{r} \tag{3.37}$$

$$R_{uv} = \frac{2a_u a_v}{a^2} - \frac{2a_{uv}}{a} - \frac{2r_{uv}}{r} \tag{3.38}$$

$$R_{\theta\theta} = \frac{4r r_{uv}}{a^2} + \frac{4r_u r_v}{a^2} + 1 \tag{3.39}$$

Which together with equation 3.32 leads to:

$$4\pi r\Phi_u^2 - \frac{2a_u r_u}{a} + r_{uu} = 0 \tag{3.40}$$

$$4\pi r\Phi_v^2 - \frac{2a_v r_v}{a} + r_{vv} = 0 \tag{3.41}$$

$$4\pi\Phi_u\Phi_v - \frac{a_u a_v}{a^2} + \frac{a_{uv}}{a} + \frac{r_{uv}}{r} = 0 \tag{3.42}$$

$$rr_{uv} + r_u r_v + \frac{a^2}{4} = 0 \tag{3.43}$$

The previous set of equations and equation 3.35 define completely the problem in the asymptotically flat case. In chapter 4 we describe the numerical set up to solve these equations.

3.3.2. $\Lambda < 0$

In order to obtain the Equations for an AdS bacground we have to add the term $\Lambda g_{\mu\nu}$ to the equations for asymptotically flat spacetime. We will be using the same form for the line element, so the wave equation is the same as equation 3.35. The remaning equations are:

$$4\pi r\Phi_u^2 - \frac{2a_u r_u}{a} + rr_{uu} = 0 \tag{3.44}$$

$$4\pi r\Phi_v^2 - \frac{2a_v r_v}{a} + rr_{vv} = 0 \tag{3.45}$$

$$4\pi\Phi_u\Phi_v - \frac{a_u a_v}{a^2} + \frac{a_{uv}}{a} + \frac{r_{uv}}{r} + \frac{3a^2}{4L^2} = 0 \tag{3.46}$$

$$rr_{uv} + r_u r_v + \frac{a^2}{4} + \frac{3a^2 r^2}{4L^2} = 0 \tag{3.47}$$

3.3.3. Scalar quantities of interest

In order to study the critical behaviour of the solution we want to be able to observe the self-similar solution described by Choptuik, so that equation 2.1 must hold. We define the proper time T on the axis $u = v$ by considering:

$$-F(r)dt^2 + F(r)^{-1}dr^2 = -a^2 dudv \tag{3.48}$$

Where $F(r)$ can be any of the functions defined by equations 3.16, 3.18, 3.22, or 3.27. The proper time on axis ($u = v$, $r = 0$) will be given by:

$$dT^2 = \frac{a^2}{F(0)} du^2 \tag{3.49}$$

Or integrating:

$$T(u) = \frac{1}{F(0)} \int_0^u a(w, w) dw \tag{3.50}$$

As can be seen from equations 3.16 and 3.22 we can take $F(0) = 1$ before black hole formation.

Another scalar quantities that will be important for us are the Hawking mass and the Ricci scalar defined by:

$$m(u, v) = \frac{r}{2} \left(1 + \frac{4 r_u r_v}{a^2} \right) \tag{3.51}$$

$$R(u, v) = -32\pi \frac{\Phi_u \Phi_v}{a^2} \tag{3.52}$$

4. Numerical Methods

In this chapter we describe the numerical methods used to solve the Einstein equations presented in chapter 3. Our basic problem is to define the initial data for the Cauchy problem and impose appropiate boundary conditions. First we simplify the system of equations 3.40 - 3.43 and 3.44 - 3.47 by following the same procedure described in [5] .

4.1. Equations

We introduce a new set of variables by:

$$c = \frac{a_u}{a}, \quad d = \frac{a_v}{a}, \quad f = r_u, \quad g = r_v, \quad \sqrt{4\pi}\Phi, \quad p = s_u, \quad q = s_v \tag{4.1}$$

and the auxiliary variables:

$$\lambda = fg + \frac{1}{4}a^2, \qquad \mu = fq + gp \tag{4.2}$$

Using this new variables we can rewrite the system of equations 3.40 - 3.43 and 3.44 - 3.47 as a set of 14 equations depending on the new variables. We have labelled them as M1 - M14 for the equations corresponding to asymptotically flat spacetime, and as A1 - A14 for the ones corresponding to AAdS spacetime.

$M1$	$a_u - ac = 0$	$A1$	$a_u - ac = 0$	(4.3)
$M2$	$a_v - ad = 0$	$A2$	$a_v - ad = 0$	
$M3$	$r_u - f = 0$	$A3$	$r_u - f = 0$	
$M4$	$r_v - g = 0$	$A4$	$r_v - g = 0$	
$M5$	$s_u - p = 0$	$A5$	$s_u - p = 0$	
$M6$	$s_v - q = 0$	$A6$	$s_v - q = 0$	
$M7$	$rp_v + \mu = 0$	$A7$	$rp_v + \mu = 0$	
$M8$	$rq_u + \mu = 0$	$A8$	$rq_u + \mu = 0$	
$M9$	$r^2c_v - \lambda + r^2pq = 0$	$A9$	$r^2c_v - \lambda + r^2pq = 0$	
$M10$	$r^2d_u - \lambda + r^2pq = 0$	$A10$	$r^2d_u - \lambda + r^2pq = 0$	
$M11$	$rf_v + \lambda = 0$	$A11$	$rf_v + \lambda + \frac{3r^2a^2}{4L^2} = 0$	
$M12$	$rg_u + \lambda = 0$	$A12$	$rg_u + \lambda + \frac{3r^2a^2}{4L^2} = 0$	
$M13$	$f_u - 2cf + rp^2 = 0$	$A13$	$f_u - 2cf + rp^2 = 0$	
$M14$	$g_v - 2dg + rq^2 = 0$	$A14$	$g_v - 2dg + rq^2 = 0$	

The system of equations M1 - M14 is similar to A1 - A14, so in the following we describe only the case of asymptotically flat spacetime. It should be understood that the procedure is the same for AAdS by changing the label M by the label A in the corresponding equation. We will stress when a distinction between the two set of equations is necessary.

Out of the 14 equations, not all are independent. First, we noticed that there are equations in both u and v for all the variables with the exception of d and q which can only evolve in the u direction, or c and p which can only evolve in the v direction. We interpret this as a characteristic of the Cauchy problem in GR, which expressed by means of the ADM formalism requires two equations to determine the spatial metric and the extrinsic curvature from one time slice to the next. The remaining equations were used as the constraint equations in the Cauchy initial surface.

The obvious choice for the initial Cauchy surface is the null surface $u = constant$ or $v = constant$. We decide to specify the initial data on $u = constant$, so we fix the evolution equations to be $M8$ and $M10$. By doing this, we eliminate all the other equations which have derivatives with respect to u. In addition, by considering the expressions for the Ricci scalar and the Hawking mass, we decide to calculate all other

variables with the exception of c. At last, we are left with equations $M2$, $M4$, $M6$, $M7$, $M11$ and $M14$ as the constraint equations, while $M8$ and $M10$ were used as the evolution equations.

The equations were integrated following the scheme outlined in [5]. Basically, we defined the initial value for q and d in $u = 0$. Then we used $M2$ and $M6$ to integrate a and s respectively. Next $M4$ and $M14$ were used to integrate r and g. Finally, $M7$ and $M11$ updated p and f. Once all variables were updated for any layer $u = constant$, $M8$ and $M10$ were used to calculate d and q in the next layer and the process is repeated layer by layer.

4.1.1. Initial and boundary conditions

As mentioned previously, initial conditions must be applied to d and q in the initial slice at $u = 0$. For the case of asymptotically flat spacetime, we would require the original metric to be Minkowski, so that $a(0, v) = 1$ and therefore $d(0, v) = 0$. On the other hand, we have freedom to choose the initial shape of the scalar field Φ, and therefore the shape of $q(0, v)$. The initial scalar field configuration was set to be:

$$\Phi(u = 0, r) = Ar^2 \exp\left(-\frac{(r - r_0)^2}{\sigma^2}\right) \tag{4.4}$$

So that $q(0, v)$ was given by:

$$q(0, v) = \exp\left(-\frac{(v - v_0)^2}{\sigma^2}\right)\left(2Av - \frac{2Av^2}{\sigma^2}(v - v_0)\right) \tag{4.5}$$

For the case of asymptotically AdS we had to consider the line element given by equation 3.26, so that $a(0, v) = \sec(v/2L)$, and $d(0, v) = (2L)^{-1}\tan(v/2L)$. For $q(0, v)$ we used the same expression in equation 4.5.

In addition we need to supply the boundary conditions at the axis $u = v$. Clearly, at the axis, $r = 0$, so $f = -g$. That also implies that $\lambda = 0$ and $\mu = 0$, so on axis $a = 2g$ and $p = q$. Finally we have to impose boundary conditions for a and s which for continuity were set to be:

$$\frac{\partial a}{\partial r} = 0 \qquad \frac{\partial s}{\partial r} = 0 \tag{4.6}$$

The previous conditions define the set up for our algorithm. The basic idea is to modify the original data by means of changing the initial perturbation $q(0, v)$.

4.1.2. Numerical integration

At this point we explain the numerical procedure used to integrate the equations M1 - M14 and A1 - A14.

The first task is to integrate the constraint equations in each slice $u = constant$. To maintain numerical accuracy we decided to follow the literature and use a fourth order Runge-Kutta method to perform the integrations [4, 35, 36]. Basically, we wrote the equations $M2$, $M4$, $M6$, $M7$, $M11$ and $M14$ in the general way:

$$Y_v = F(Y, v) \tag{4.7}$$

Then we define the size step dv so that v becomes a discrete variable $v_i = i \times dv$ and we intend to calculate the value $Y_i = Y(v_i)$ given the initial data Y_0. Once the value for Y_i is known, the value of Y_{i+1} is calculated by:

$$\begin{aligned} Y_{i+1} &= Y_i + \frac{k_1}{6} + \frac{k_2}{3} + \frac{k_3}{3} + \frac{k_4}{6} \\ k_1 &= dvF(Y_i, v_i) \\ k_2 &= dvF(Y_i + k_1/2, v_i + dv/2) \\ k_3 &= dvF(Y_i + k_2/2, v_i + dv/2) \\ k_4 &= dvF(Y_i + k_3, v_i + dv) \end{aligned} \tag{4.8}$$

The evolution equations are treated in a somewhat different manner considering the fact that other than the value of the variables at the previous layer, we can also use the value in a previous step in v. For simplicity we will use $h = dv$. Figure 4.1 shows a diagram of the procedure used to integrate the evolution equations.

We use a predictor corrector method to calculate the values of d and q in the point $n(u, v)$ given that we know the value of all the other variables in the points $w(u, v - h)$ and $e(u - h, v)$. First, we wrote all the equations in the form of:

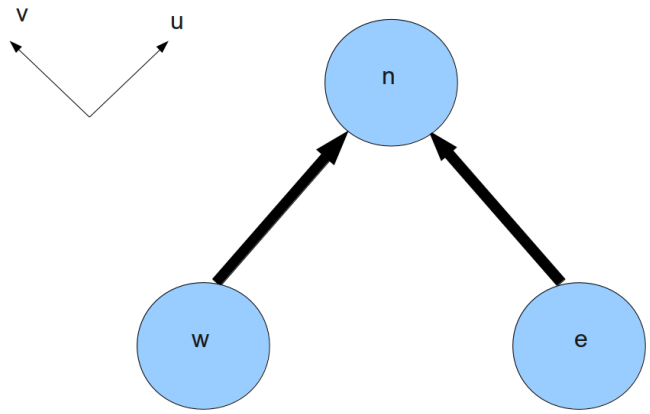

Figure 4.1.: Basic cell used for the evolution scheme. The information in the points w(u,v-h) and e(u-h,v) is used to calculate the solution in the point n(u,v).

$$Y_v = F(Y, Z) \tag{4.9}$$
$$Z_u = G(Y, Z)$$

Clearly, Z represents q or d while Y is any of the remaining variables. First, we update the values of Y and Z for an intermediate point m using the explicit step given by:

$$Z(m) = Z(e) + hG\left(Y(e), Z(e)\right) \tag{4.10}$$
$$Y(m) = Y(w) + \frac{1}{2}h\left(F\left(Y(w), Z(w)\right) + F\left(Y(m), Z(m)\right)\right) \tag{4.11}$$

For the Y variables, equation 4.11 is solved explicitly to find $Y(m)$ and the equations are shown in Appendix B.

Next, we calculate the values for the Z variables by:

$$Z(n) = \frac{1}{2}\left(Z(m) + Z(e) + hG\left(Y(m), Z(m)\right)\right) \tag{4.12}$$

Boundary conditions

With the exception of equations 4.6 all the other boundary counditions are straightforward to implement.

On axis we can approximate the derivatives in 4.6 with a second order accurate forward difference equation:

$$\left(\frac{\partial a}{\partial r}\right)_{u=v} = \frac{-a(u-2h,u+2h)+4a(u-h,u+h)-3a(u,u)}{2\sqrt{2}h} \tag{4.13}$$

So that the boundary conditions for a and s become:

$$a(u,u) = \frac{1}{3}\left(4a(u-h,u+h)-a(u-2h,u+2h)\right) \tag{4.14}$$

$$s(u,u) = \frac{1}{3}\left(4s(u-h,u+h)-s(u-2h,u+2h)\right) \tag{4.15}$$

In the case of AdS we should also provide the boundary conditions at null infinity. However, we will focus on the gravitational collapse before any reflection in the AdS boundary, so that these conditions can be neglected.

The whole procedure for solving the Einstein-scalar system can be summarized as:

1. Define the initial values for d and q in the surface $u = 0$.
2. Integrate the constraint equations ($M2$, $M4$, $M6$, $M7$, $M11$ and $M14$) on the first slice ($u = 0$) by using a fourth order Runge-Kutta method (Equation 4.8).
3. Impose boundary conditions on axis ($u = v$) and calculate the value of d and q by using the predictor corrector method (Equation 4.12).
4. Calculate the values for the remaining variables by integrating the constraint equations once.
5. Repeat steps 3 and 4 iteratively moving away from the axis and from layer to layer.

4.2. Black hole creation

Our main goal is to study the behaviour of the solution near the threshold of black hole formation. To do that, we varied the amplitude A of the initial pulse given by equation 4.4. We expect that for values of A smaller than the critical value A^* the pulse will be reflected at the origin and will disperse towards infinity. On the contrary, for $A > A^*$ the solution will collapse to form a black hole. We say that a black hole has began to form when a closed trapped surface appears, which we identify with the formation of an apparent horizon (AH). In our system of coordinates, the AH is related to the condition $g = 0$.

Explicitly, we defined that an AH has formed when $g < 10^{-4}$. Our choice of coordinates is stable inside the AH and it begins to diverge when it approaches the singularity at $r = 0$.

4.3. Control quantities

In order to secure that our integration method is numerically stable we decided to use some of the equations which were not used for the integration as control equations. Due to the importance of g in signaling the formation of an apparent horizon, we chose equations $M12$ and $A12$ as our control equations for asymptotically flat and AAdS cases respectively.

5. Results

In this section we present the results obtained by solving the system of equations $M1$ - $M14$ and $A1$ - $A14$. We modified the amplitude A in the initial perturbation to find the value A^* in the threshold between black hole formation and dispersion to infinity. In both cases, we used a grid with 4000 points and a step size of 0.0025. We found that this choice is sufficient to observe the self-similar behaviour of the critical solution. The constraint equations A12 and M12 are shown in appendix C.

5.1. Asymptotically flat spacetime

The major goal of our simulation in asymptotically flat spacetime is to check the consistency of the method and reproduce the results known about the existence of a critical solution in the threshold of black hole formation. We began with a perturbation given by the shape of $d(0, v)$ in equation 4.5. The values $v_0 = 2$ and $\sigma = 1/\sqrt{2}$ were fixed, so we used A to form a one parameter family of initial data as required by the work of Choptuik. As expected, we found that for values of $A < A^*$ the solution reflected on the origin and lead to dispersion. Figure 5.1 shows the evolution of the scalar field for a subcritical evolution. The original perturbation bounces at the origin and is dispersed to future null infinity.

On the contrary, if we choose a high enough value for A, the solution will eventually collapse which we identified by the formation of an apparent horizon. Figure 5.2 shows a density plot of s as a function of u and v. The simulation shows the formation of a spacelike singularity at $r = 0$. It is interesting to put figure 5.2 in context with the full Penrose diagram of the spacetime. Figure 5.3 shows a schematic representation of the full Penrose diagram for an asymptotically flat spacetime with the formation of a Schwarzschild black hole. The region inside the dotted lines is just a portion of the full diagram, and represents the region covered by our coordinates in the simulation.

In figure 5.4 we plot r and g as a function of v for $u = 1.1$ and for $u = 1.9$. In this case, the formation of the apparent horizon occurs at $u = 1.8625$. After the formation

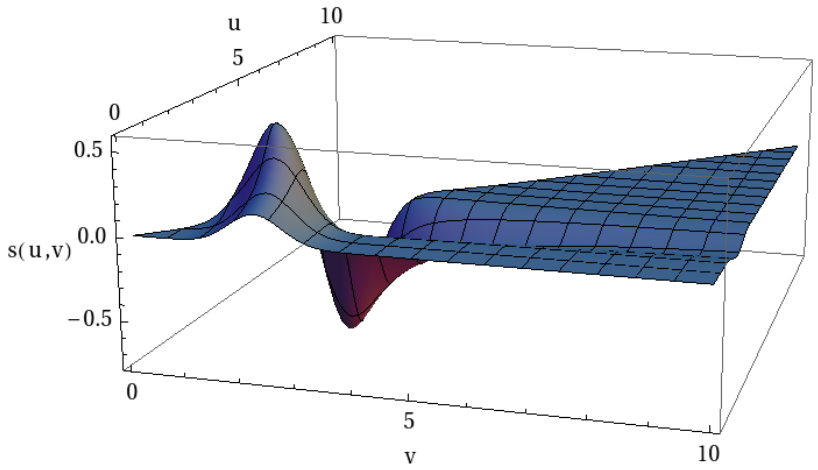

Figure 5.1.: Evolution of the scalar field s for a subcritical solution as a function of u and v. The initial incoming field bounces at the origin ($u = v$) and then is dispersed to infinity.

of the apparent horizon, r and g diverge. For plotting purposes, in all our plots we set the value of the variables to be equal to -1 when they diverge. One can see that after the apparent horizon at $g = 0$ is formed, r is not a growing function of v anymore and a closed trapped surface has formed.

In figure 5.5 we show a plot of the metric coefficient a. Before the formation of the AH it remained close to 1 but when the horizon forms it grows until our code breaks (which in the figure corresponds to the values of $a = -1$). Interestingly, the maximum value of a shows a self-similar behaviour.

Next we studied the properties of the critical solution. For that we had to find the value A^* such that if $A < A^*$, the original perturbation is dispersed to future null infinity, and if $A > A^*$ a black hole was formed. To do that, we began with two values A^+ and A^- which were known to be supercritical and subcritical respectively. Next we defined

$$\hat{A} = \frac{A^+ + A^-}{2}$$

and check whether it was a subcritical or a supercritical solution. As usual, the variable g was used to signal whether an apparent horizon was formed or not. $\hat{A}$ then replaces

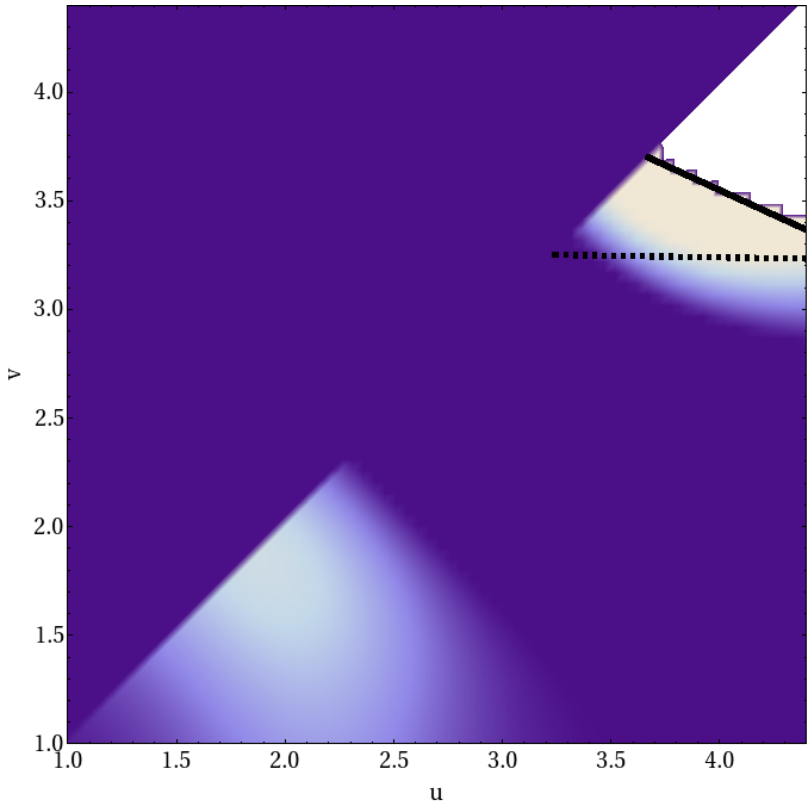

Figure 5.2.: Density plot of the scalar field s for a supercritical solution. In the region in white our code breaks due to the collapse of the scalar field. One can distinguish the formation of the spacelike singularity at the origin (full line) and the AH (dotted line).

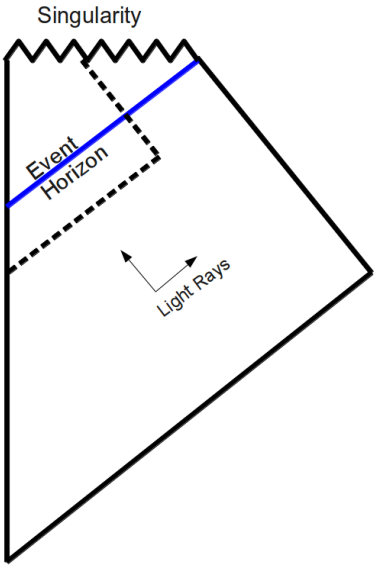

Figure 5.3.: Penrose diagram of a Schwarzschild type black hole formation. The region inside the dotted lines represents a portion of the spacetime which would be covered in our simulation.

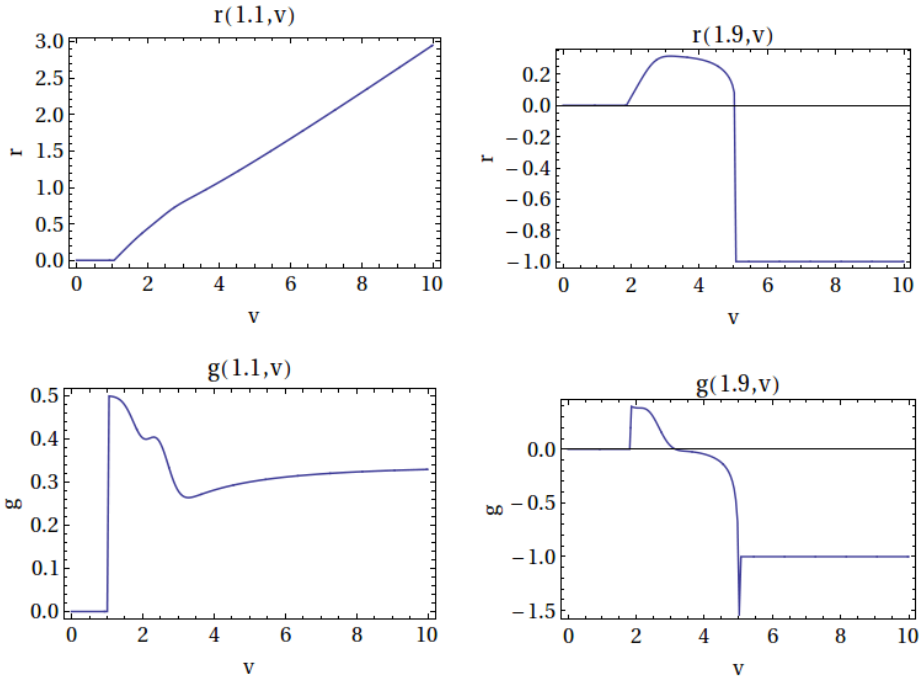

Figure 5.4.: Plot of the variables r and g before the formation of the AH (left) and after (right) for a supercritical solution.

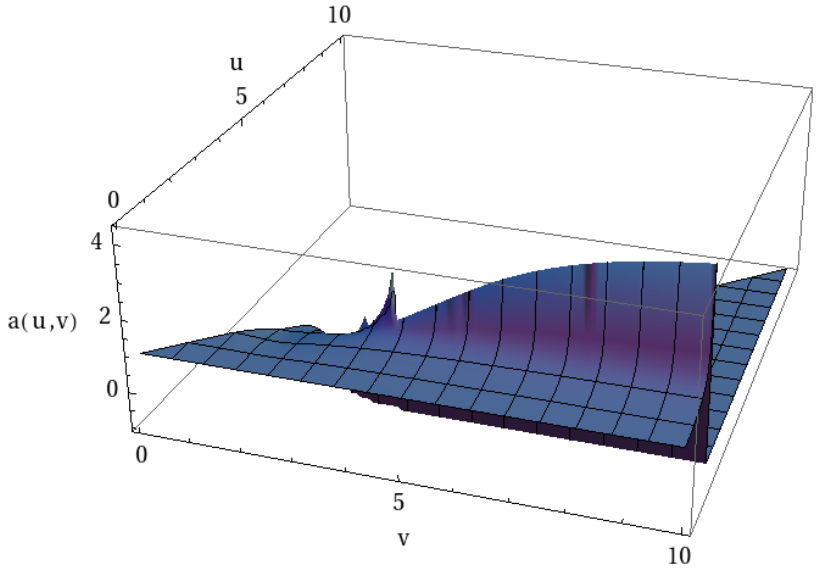

Figure 5.5.: Evolution of the metric coefficient a in a supercritical solution as a function of u and v. When the AH is formed, a begins growing exponentially until our code breaks down. The maximum value before it breaks down suggest a self-similar behaviour for the function a in the AH.

A^+ or A^- and the procedure was repeated. The refinement on which this procedure can be done is dependent on the minimum value of g that one can pick as the condition for AH formation, which in our case is 10^{-4}. For lower values of g the AH formed and we were not able to detect it.

We were able to determine the parameter A^* to about one part in 10^{10}. In figure 5.6 we plot a subcritical solution close to the critical solution and we observed the self-similar behaviour reported in the literature. With our fixed grid, we were able to clearly observe up to three oscillations of the scalar field.

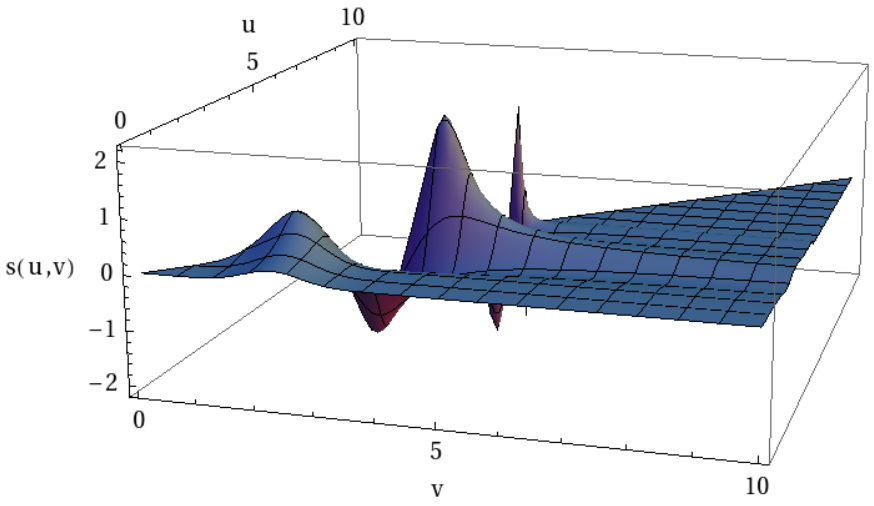

Figure 5.6.: Evolution of the scalar field s in a slightly subcritical solution as a function of u and v. The appearance of the oscillations is an indication of the existence of the self-similar critical solution.

The scale echoing parameter Δ defined in equation 2.1 should be observed when we use the proper time coordinate T defined in equation 3.50. If we define the proper time T^* when the singularity is formed in the critical solution, we should have that Δ is the period of oscillations in the coordinate $\tau = -\ln(T^* - T)$. We obtained a value of $\Delta = 3.02$, in contrast to the value of 3.44 reported in [2, 5]. The main differences can always be attributed to the fact that the determination of T^* has great uncertainty and the fact that we need higher resolution to study the late peaks in the oscillation of the critical solution. In particular, in figure 5.7 we plot the scalar field s as a function of T on the axis and we observe three peaks which show the symmetry described by Choptuik,

but the last peak has a much lower resolution, so we have a great uncertainty in the determination of T^* and consequently the period of the oscillations Δ. The blue line is a slightly subcritical solution and the red line is a slightly supercritical solution. The fact that both solutions look very much alike before collapse or dispersion is a proof of the picture of universallity depicted in figure 2.1.

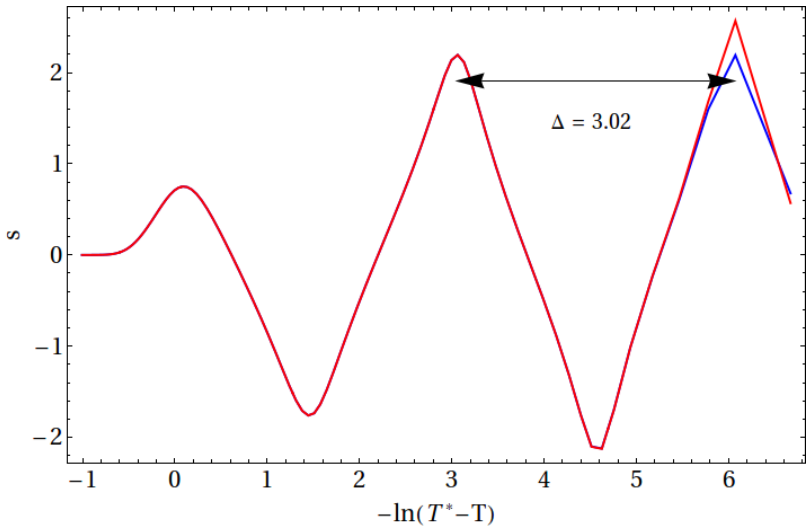

Figure 5.7.: Plot of the field s vs $\ln(T^* - T)$ on axis. The solution for a slightly subcritical solution is plot in blue and for a slightly supercritical solution in red. The observed period of the oscillations is 3.02.

The self-similar behaviour is also observed in the metric coefficient a as can be seen in figure 5.8. The number of oscillations in a is the double as it is a quadratic function in the derivative of Φ. We also plot the Ricci scalar given by equation 3.52. On axis, it has the form:

$$R(u,u) = -32\pi \frac{d^2\Phi}{dT^2} \tag{5.1}$$

For the critical solution we expect it to grow according to $\exp(2\Delta)$ after each oscillation. Figure 5.9 shows a logarithmic plot of R, and we observe the predicted growth on R. We used the growth of R to estimate the value of Δ and we find it to be of 3.23, which is closer to the expected value of 3.44.

Finally, we want to study the mass scaling law from equation 2.8. To do that, we chose several supercritical values for A and used equation 3.51 to determine the black hole mass at the point where the AH begins to form. The plot in figure 5.10 shows a linear dependence between the logarithm of the black hole mass as a function of $\ln(A - A^*)$.

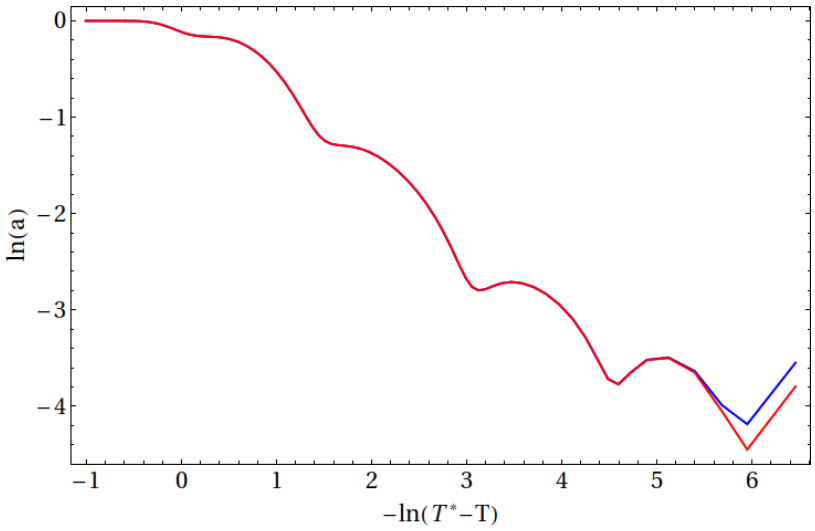

Figure 5.8.: Plot of the logarithm of the metric coefficient a as a function of $\ln(T^* - T)$. The plots correspond to the same solutions shown in figure 5.7

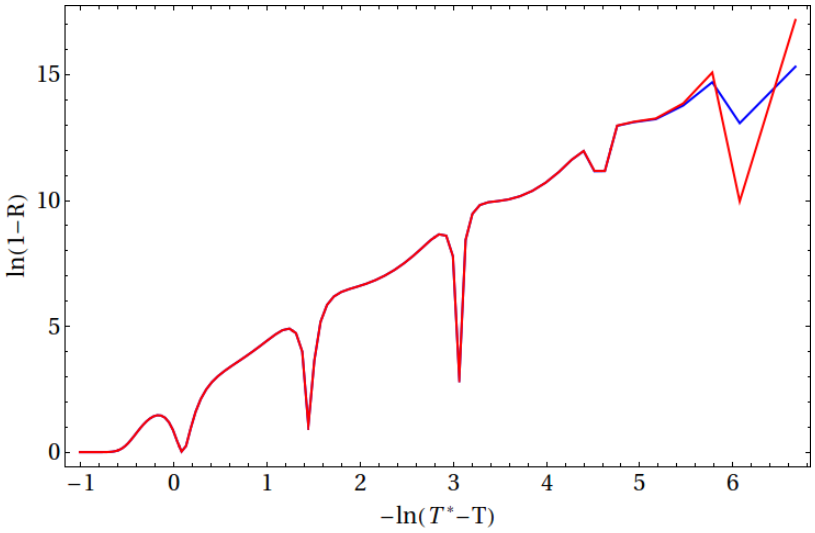

Figure 5.9.: Plot of the logarithm of the Ricci scalar R as a function of $\ln(T^* - T)$. As expected, R grows as $\exp(2\Delta)$ for each oscillation. The plots correspond to the same solutions shown in figure 5.7

The slope of the curve is then the exponent γ in equation 2.8. The value of $\gamma = 0.371$ is in agreement with the value found by Choptuik of 0.36 and by Hamade and Stewart of 0.374.

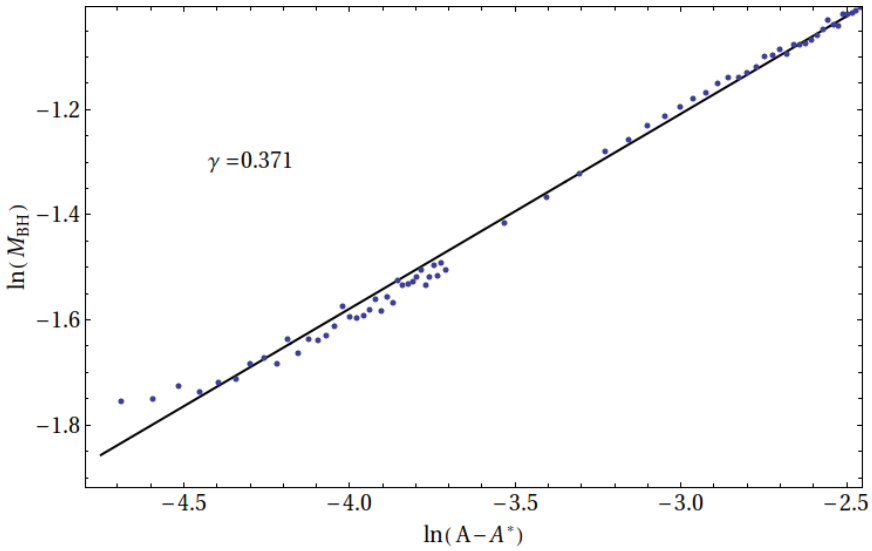

Figure 5.10.: Plot of the logarithm of the black hole mass M for supercritical solutions as a function of $\ln(A - A^*)$. The plot clearly shows a linear dependence which is a result of the mass scaling law for near critical solutions.

5.2. Asymptotically AdS spacetime

For the AAdS we proceeded in a similar way to the one described for the asymptotically flat spacetime case. We considered the case of collapse before any reflection in the AdS boundary. As discussed previously, Bizon et. al [4] have shown that any initial perturbation would lead to black hole formation if one waits for long enough. However, they found that the critical behaviour still appears if one defines the threshold for black hole formation before n reflections in the boundary. Moreover, the critical solution is the same as the one found by Choptuik for asymptotically flat spacetimes. For our purpose, it is then sufficient to consider the case where the black hole formation occurs before any reflection in the AdS boundary. Previous works used the same approach and determined the critical parameters when the collapse ocurs before any reflection, for BTZ black holes in AdS_3 [36], and for Schwarzschild black holes in AdS_5 [35].

In order to compare our results with the case of asymptotically flat spacetime, we used the same domain D for our simulation $D = \{(u, v)/ \quad 0 \leq u, v \leq 10, \quad u \leq v\}$. The value of L was chosen so that the AdS boundary is outside our domain. From equation

3.26 we must have $L \geq 10/\pi$. Three values of L were used: $L = 4$, $L = 10$, $L = 100$, corresponding to $\Lambda = -0.1875$,$\Lambda = -3.333 \times 10^{-2}$ and $\Lambda = -3.333 \times 10^{-4}$ respectively. The original perturbation was kept the same with $v_0 = 2$ and $\sigma = 1/\sqrt{2}$. Figure 5.11 shows a scheme of the simulations. The region inside the black triangle is D, the domain of our simulation. The three lines at $L = 4$, $L = 10$ and $L = 100$ represent the timelike boundary at null infinity. By choosing higher values of L, the boundary moves farther appart from the axis $u = v$ and in the limit $L \to \infty$ we would recover the asymptotically flat case.

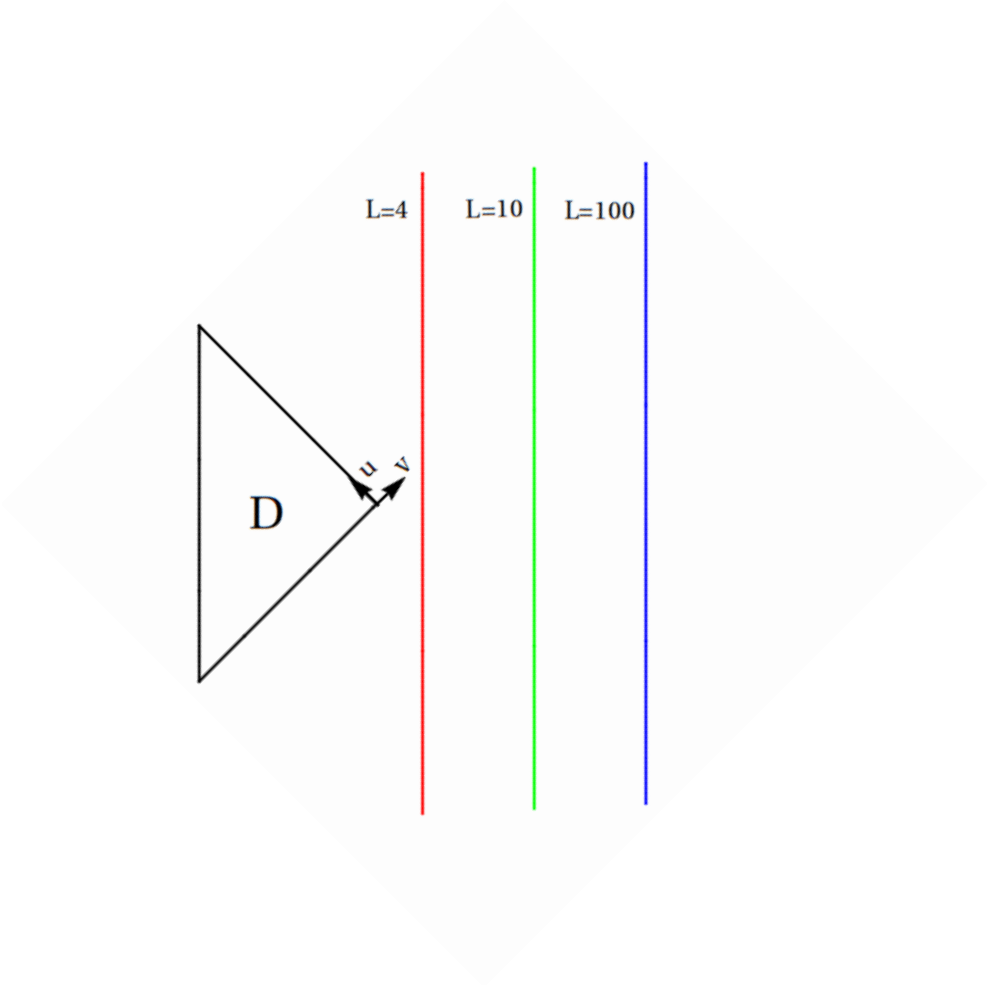

Figure 5.11.: Scheme of the AdS boundary as a function of L. For larger L, the AdS boundary displaces further apart from the axis at $u = v$. In the limit $L \to \infty$ we should recover asymptotically flat spacetime.

For the three values of L we followed the same procedure as described in asymptotically flat spacetime to find the value of the parameter A^* in the threshold of black hole

Table 5.1.: Amplitude A^* in the critical solution for various values of L (Up to ten decimal places).

	A^*
$L = 4$	0.0501040890
$L = 10$	0.0511476329
$L = 100$	0.0513385877
$L = \infty$	0.0513408203

formation. In table 5.1 we report the values found for each case up to 10 decimal places. The value corresponding to $L = \infty$ is the value found for asymptotically flat spacetime. It is interesting to note that the critical parameter asymptotes rapidly towards its flat space value.

For values of $A < A^*$ we observed qualitatively the same behaviour of asymptotically flat spacetime where the ingoing pulse is reflected at the axis $u = v$. As mentioned earlier, we restrict our simulation to perturbations which collapse before any reflection in the AdS boundary at $v - u = \pi L$. For the supercritical case $A > A^*$ a black hole was formed and we observed the formation of an apparent horizon signalled by $g = 0$ just as the case shown in figure 5.2. Figure 5.12 shows a plot of r and g for a supercritical solution in which the AH forms at $u = 1.8575$. Qualitatively we observe the same behaviour of the asymptotically flat case, and it is clear to see the formation of a closed trapped surface from the plots at $u = 1.9$.

We are more interested in the critical behaviour. At the critical point A^* the scalar field shows the same self-similar behaviour as the one observed in the asymptotically flat case. With our resolution, we observed a similar picture to the one shown in figure 5.6 for the three different values of L.

Figure 5.13 shows a plot of the scalar field s as a function of proper time T for the three different values of L. The value of Δ was estimated from the period of oscillation of s and we found it to be of 2.98 for $L = 10$ and $L = 100$, and of 2.94 for $L = 4$. The difference between them and the universal value of 3.44 again is attributed to our lack of resolution near the formation of the singularity. Just as the case of asymptotically flat spacetime, the last peak has a much lower resolution, and therefore we obtain larger errors in the determination of Δ. We further found the same oscillatory pattern for a and R as can be seen in figures 5.14 and 5.15. The oscillations in R where used to estimate Δ and we found a value of 3.24.

Finally we studied the mass scaling law for AAdS. As expected, the critical exponent

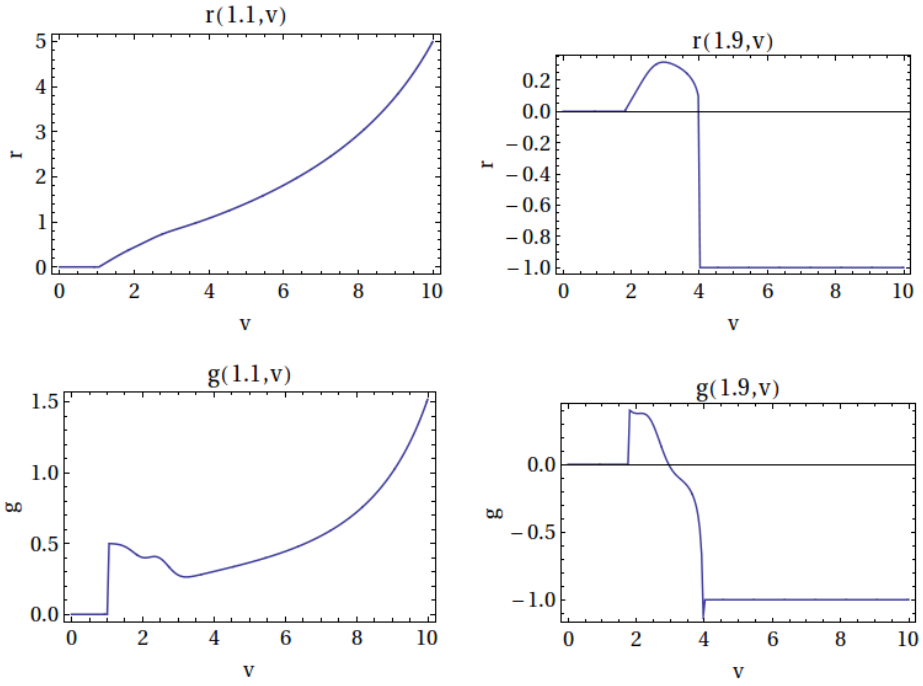

Figure 5.12.: Plot of the variables r and g before the formation of the AH (left) and after (right) for a supercritical solution in the case $L = 4$.

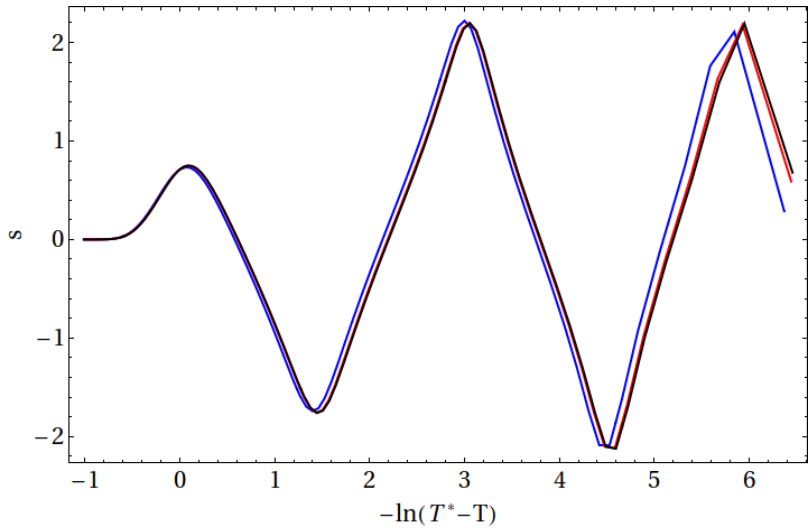

Figure 5.13.: Plot of the field s vs $\ln(T^* - T)$ on axis. The solution for $L = 4$, $L = 10$ and $L = 100$ are ploted in blue, red and black respectively. The period of the oscillations is 2.98 for $L = 10$ and $L = 100$, and 2.94 for $L = 4$.

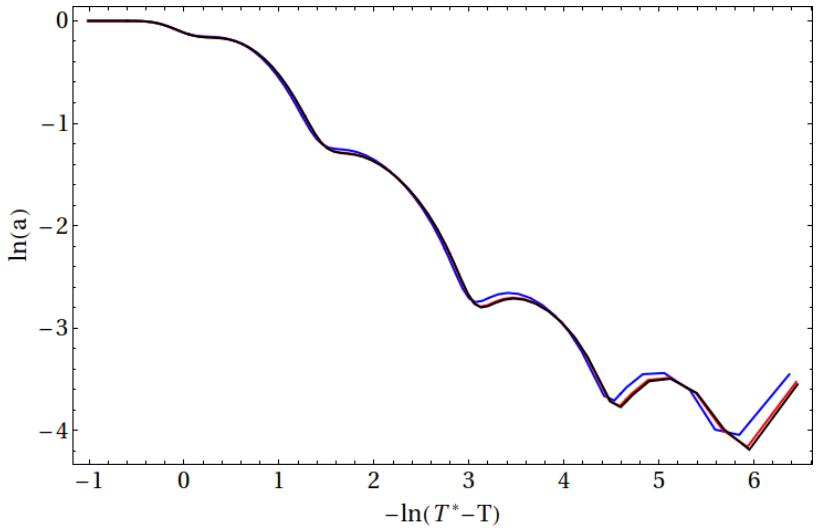

Figure 5.14.: Plot of the logarithm of the metric coefficient a as a function of $\ln(T^* - T)$. The plots correspond to the same solutions shown in figure 5.13

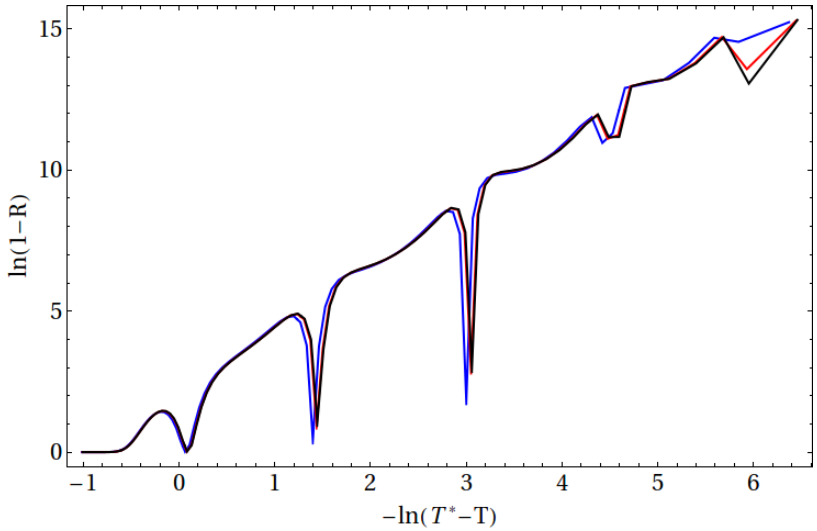

Figure 5.15.: Plot of the logarithm of the Ricci scalar R as a function of $\ln(T^* - T)$. As expected, R grows as $\exp(2\Delta)$ for each oscillation. The plots correspond to the same solutions shown in figure 5.13

γ is the same as the asymptotically flat case. Figure 5.16 shows a plot of $\ln(M_{BH})$ as a function of $\ln(p - p^*)$ for the three cases considered.

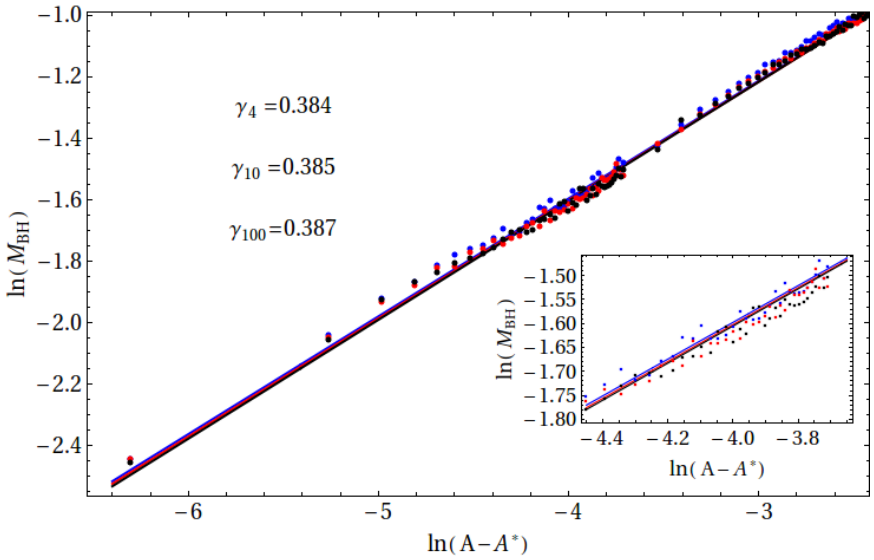

Figure 5.16.: Plot of the logarithm of the black hole mass M for supercritical solutions as a function of $\ln(A - A^*)$. The plot clearly shows a linear dependence which is a result of the mass scaling law for near critical solutions. $L = 4$, $L = 10$ and $L = 100$ are depicted in blue, red and black respectively.

Figures 5.13, 5.15, 5.14 and 5.16 all suggest that the critical solution is the same one found by Choptuik for the flat case. The fact that the critical solution is the same, even for the case of $L = 4$ reflects the fact that the properties of gravitational collapse arise from the local structure of spacetime, so that in the vicinity of the singularity, the effect of the negative cosmological constant is negligible. However, it is remarkable that the negative cosmological constant has a definite effect on gravitational collapse when the large structure of the spacetime is considered. In particular, by considering the existence of a timelike boundary at null infinity, AdS turns instable for an arbitrarily small perturbation.

We decided to further study the dependance of the amplitude A^* and the AdS radius L. We kept the same profile for the original perturbation, so that our results are valid for the particular case considered in this work. We estimated A^* up to one part in 10^7 for a total of 10 different values of L. The results are shown in table 5.2 and a plot of A^* as a function of L is shown in Figure 5.17. A^* asymptotes rapidly towards the asymptotically flat spacetime value. Presumably, the relation will be some exponential equation of the form $A^* = A^*_\infty(1 - \exp(f(L, v_0, \sigma))$, where A^*_∞ is the amplitude in asymptotically flat spacetime, and $f(L, v_0, \sigma)$ is an undetermined function of the AdS radius L, and possibly

Table 5.2.: Amplitude A^* in the critical solution for various values of L (Up to seven decimal places).

	A^*
$L = 4$	0.0501041
$L = 5$	0.0505578
$L = 8$	0.0510383
$L = 10$	0.0511476
$L = 20$	0.0512925
$L = 40$	0.0513285
$L = 100$	0.0513386
$L = 200$	0.0513400
$L = \infty$	0.0513408

depending on the parameters v_0 and σ.

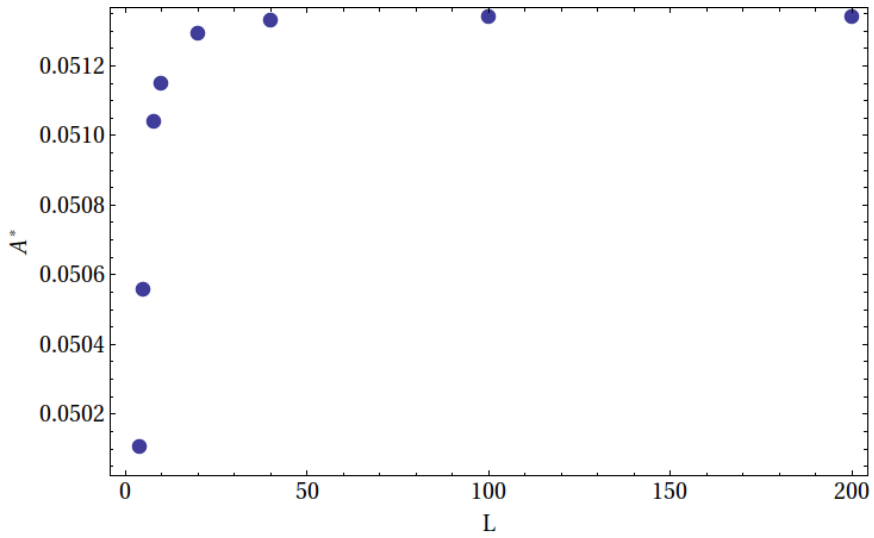

Figure 5.17.: Plot of the parameter A^* as a function of L.

6. Conclusions

The aim of this thesis was to study the critical phenomena at the threshold of black hole formation for the gravitational collapse of the massless scalar field in both asymptotically flat and asymptotically AdS spacetime using double null coordinates. We started by writing the Einstein-scalar equations and implemented an integration algorithm based on Hamade and Stewarts procedure for asymptotically flat spacetime [5]. The same algorithm was used to integrate the system of equations for AAdS and we observed the critical phenomena at the threshold of black hole formation. For a small amplitude of the initial perturbation, the incoming wave was reflected at the origin and dispersed to infinity. In the case of AAdS we limited our simulation to a subset of the whole spacetime which did not include the time-like boundary at future null infinity.

By fine tuning the initial data to the threshold of black hole formation we found a critical solution with the self-similar properties as the one described originally by Choptuik. We observed up to three oscillations for the scalar field. The metric coefficient a and the Ricci scalar curvature R showed similar periodic behaviour. Our results for the universal parameters Δ and γ agree with the ones reported in literature up to our computational resources. The value of Δ was obtained by measuring the periodicity of the scalar field s with respect to $\ln(T^* - T)$, and also by considering the expected exponential growth of the Ricci scalar R on axis. By doing that, we obtained values of 3.02 and 3.23 respectively, which are slightly lower than the value of 3.44 reported in the literature. We attribute the difference to the fact that the determination of Δ depends on finding precisely the proper time T^* when the singularity forms in the critical solution. Our simulations were performed on a fixed grid, which is not adapted to the high resolution required to investigate the critical solution when we approach the singularity.

For supercritical solutions we plotted the black hole mass at the apparent horizon and we found the black hole mass scaling law with a parameter γ of 0.371. In this case, our result agrees with the values of 0.36 - 0.37 reported in the literature.

In order to compare our results for AAdS and asymptotically flat spacetime, we used the same domain for the grid in our simulation, and the same gaussian profile for the

initial perturbation. We considered three values for the AdS radius, $L = 4$, $L = 10$, $L = 100$. In the three cases we found the same critical parameters as in asymptotically flat spacetime. In the same way as we did for asymptotically flat spacetime, we measured the period of the oscillations of the scalar field s on axis, and obtained a value of 2.98 for Δ when $L = 10$ and $L = 100$, and a value of 2.94 when $L = 4$. The result obtained by measuring the growth of R was 3.24, which is much closer to the actual value of 3.44.

By fixing our simulation domain and the shape of the initial perturbation, we studied the behaviour of the amplitude A^* in the critical solution for our particular family of initial data. Our results showed that the amplitude of the critical solution A^* asymptotes rapidly towards its value in flat spacetime. It is worth mentioning that the particular shape of the curve is valid for our particular choice of initial data, and should not be taken as a universal behaviour unless shown to be the same in different conditions.

6.1. Future work

A limitation of our algorithm is the lack of resolution near the formation of the singularity. Such problem can be addressed by using a mesh refinement algorithm to increase the resolution of the grid near the singularity. By using such method, we would expect to observe a larger number of oscillations in the critical solution.

In addition, our algorithm for AdS can be extended by considering the time-like boundary as part of the simulation domain. In our case, we limited our study to solutions which collapse before any reflection in the AdS boundary. Appropiate boundary conditions should be imposed to consider the case where the perturbation reaches null infinity and is reflected to the origin before collapsing. In such case we would expect to reproduce the results obtained by Bizon with a different coordinate system [4].

Bibliography

[1] R. Narayan, New J.Phys. **7**, 199 (2005), gr-qc/0506078.

[2] M. W. Choptuik, Phys. Rev. Lett. **70**, 9 (1993).

[3] J. M. Maldacena, Adv.Theor.Math.Phys. **2**, 231 (1998), hep-th/9711200.

[4] P. Bizon and A. Rostworowski, Phys.Rev.Lett. **107**, 031102 (2011), 1104.3702.

[5] R. S. Hamade and J. M. Stewart, Class.Quant.Grav. **13**, 497 (1996), gr-qc/9506044.

[6] M. W. Choptuik, E. W. Hirschmann, and S. L. Liebling, Phys. Rev. D **55**, 6014 (1997).

[7] R. M. Wald, (1997), gr-qc/9710068.

[8] J. M. Martin-Garcia and C. Gundlach, Phys.Rev. **D59**, 064031 (1999), gr-qc/9809059.

[9] C. Gundlach, Phys.Rev. **D57**, 7075 (1998), gr-qc/9710066.

[10] M. D. Roberts, Gen.Rel.Grav. **21**, 907 (1989).

[11] P. Bizon, T. Chmaj, and B. G. Schmidt, Phys.Rev.Lett. **95**, 071102 (2005), gr-qc/0506074.

[12] D. Garfinkle, R. B. Mann, and C. Vuille, Phys.Rev. **D68**, 064015 (2003), gr-qc/0305014.

[13] C. R. Evans and J. S. Coleman, Phys.Rev.Lett. **72**, 1782 (1994), gr-qc/9402041.

[14] D. W. Neilsen and M. W. Choptuik, Class.Quant.Grav. **17**, 761 (2000), gr-qc/9812053.

[15] G. Rein, A. D. Rendall, and J. Schaeffer, Phys.Rev. **D58**, 044007 (1998), gr-qc/9804040.

[16] I. Olabarrieta and M. W. Choptuik, Phys.Rev. **D65**, 024007 (2002), gr-qc/0107076.

[17] C. Gundlach, Phys.Rev. **D55**, 695 (1997), gr-qc/9604019.

[18] R. S. Hamade, J. H. Horne, and J. M. Stewart, Class.Quant.Grav. **13**, 2241 (1996), gr-qc/9511024.

[19] M. W. Choptuik, T. Chmaj, and P. Bizon, Phys.Rev.Lett. **77**, 424 (1996), gr-qc/9603051.

[20] C. Gundlach and J. M. Martin-Garcia, Living Rev.Rel. **10**, 5 (2007), 0711.4620.

[21] C. Lechner, J. Thornburg, S. Husa, and P. C. Aichelburg, Phys.Rev. **D65**, 081501 (2002), gr-qc/0112008.

[22] P. R. Brady, C. M. Chambers, and S. M. Goncalves, Phys.Rev. **D56**, 6057 (1997), gr-qc/9709014.

[23] T. Hara, T. Koike, and S. Adachi, (1996), gr-qc/9607010.

[24] J. M. Martin-Garcia and C. Gundlach, Phys.Rev. **D68**, 024011 (2003), gr-qc/0304070.

[25] P. R. Brady and M. J. Cai, p. 689 (1998), gr-qc/9812071.

[26] S. Hod and T. Piran, Phys.Rev. **D55**, 3485 (1997), gr-qc/9606093.

[27] C. Gundlach and J. M. Martin-Garcia, Phys.Rev. **D54**, 7353 (1996), gr-qc/9606072.

[28] M. W. Choptuik, E. W. Hirschmann, S. L. Liebling, and F. Pretorius, Phys.Rev. **D68**, 044007 (2003), gr-qc/0305003.

[29] M. W. Choptuik, E. W. Hirschmann, S. L. Liebling, and F. Pretorius, Phys.Rev.Lett. **93**, 131101 (2004), gr-qc/0405101.

[30] S. A. Hartnoll, C. P. Herzog, and G. T. Horowitz, Phys.Rev.Lett. **101**, 031601 (2008), 0803.3295.

[31] J. McGreevy, Adv.High Energy Phys. **2010**, 723105 (2010), 0909.0518.

[32] S. Bhattacharyya and S. Minwalla, JHEP **0909**, 034 (2009), 0904.0464.

[33] V. Balasubramanian *et al.*, Phys.Rev.Lett. **106**, 191601 (2011), 1012.4753.

[34] D. Garfinkle and L. A. Pando Zayas, Phys.Rev. **D84**, 066006 (2011), 1106.2339.

[35] D. Garfinkle, L. A. Pando Zayas, and D. Reichmann, JHEP **1202**, 119 (2012), 1110.5823.

[36] F. Pretorius and M. W. Choptuik, Phys.Rev. **D62**, 124012 (2000), gr-qc/0007008.

[37] U. H. Danielsson, E. Keski-Vakkuri, and M. Kruczenski, JHEP **0002**, 039 (2000), hep-th/9912209.

[38] V. Husain and M. Olivier, Class.Quant.Grav. **18**, L1 (2001), gr-qc/0008060.

[39] M. Banados, C. Teitelboim, and J. Zanelli, Phys.Rev.Lett. **69**, 1849 (1992), hep-th/9204099.

[40] H. Friedrich and A. D. Rendall, Lect.Notes Phys. **540**, 127 (2000), gr-qc/0002074.

[41] D. R. Brill, J. Louko, and P. Peldan, Phys.Rev. **D56**, 3600 (1997), gr-qc/9705012.

[42] O. Aharony, S. S. Gubser, J. M. Maldacena, H. Ooguri, and Y. Oz, Phys.Rept. **323**, 183 (2000), hep-th/9905111.

A. Anti de-Sitter spacetime

Anti de-Sitter (AdS) spacetime is the name given to the maximally symmetric solution of the Einstein equations with a negative cosmological constant Λ.

$$G_{\mu\nu} + \Lambda g_{\mu\nu} = 0 \qquad \Lambda < 0 \tag{A.1}$$

In 4 dimensions, it can be represented as the hyperboloid:

$$x^2 + y^2 + z^2 - u^2 - v^2 = -L^2 \tag{A.2}$$

Where the cosmological constant Λ is written in terms of L as:

$$\Lambda = -3/L^2 \tag{A.3}$$

The causal structure of AdS_4 is induced by the restriction of the metric in $\mathbb{R}^5$ given by:

$$ds^2 = dx^2 + dy^2 + dz^2 - du^2 - dv^2 \tag{A.4}$$

To understand the general properties of AdS it suffices with studying the case where we set $\Lambda = -3$ so that it is represented by the cuadric:

$$x^2 + y^2 + z^2 - u^2 - v^2 = -1 \tag{A.5}$$

Then we can define a new set of coordinates (ρ, t, θ, ϕ):

$$x = \sinh(\rho)\sin(\theta)\cos(\phi) \tag{A.6}$$
$$y = \sinh(\rho)\sin(\theta)\sin(\phi) \tag{A.7}$$
$$z = \sinh(\rho)\cos(\theta) \tag{A.8}$$
$$u = \cosh(\rho)\cos(t) \tag{A.9}$$
$$v = \cosh(\rho)\sin(t) \tag{A.10}$$

Such that the line element is now:

$$ds^2 = -\cosh^2\rho dt^2 + d\rho^2 + \sinh^2\rho d\Omega^2 \tag{A.11}$$

As the coordinate t is periodic, anti de-Sitter spacetime has closed time-like curves and it has the topology of $\mathbb{S}^1 \times \mathbb{R}^3$. One way to avoid this and maintain causallity is by going to the covering space for AdS which has the topology of $\mathbb{R}^4$. For all practical applications it will be assumed we refer to the universal covering.

By using the change of variable:

$$\tan\Psi = \sinh\rho \tag{A.12}$$

The metric in A.13 becomes:

$$ds^2 = \frac{1}{\cos^2\Psi}\left(-dt^2 + d\Psi^2 + \sin^2\Psi d\Omega^2\right) \tag{A.13}$$

From this its clear that the anti de-sitter metric is conformally related to a subset of the Einstein universe which has the topology of $\mathbb{R}^1 \times \mathbb{S}^3$. The boundary on $\Psi = \pi/2$ has the topology of $\mathbb{R}^1 \times \mathbb{S}^2$ and it is a time-like surface. To understand the implications of this, we can solve the equations for a lightlike geodesic ($ds^2 = 0$) moving radially outwards from the origin at $\Psi = 0$ towards the boundary at $\Psi = \pi/2$. Using the conformally compactified metric from A.13 we get to the conclusion that:

$$d\theta = 0 \wedge d\phi = 0 \quad \rightarrow \quad dt = d\Psi \quad \rightarrow \quad t = \Psi \tag{A.14}$$

So, a light ray emitted at $\Psi = 0$ will reach null infinity in a finite time given by

$t = \pi/2$. Because of this fact, the Cauchy problem can not be properly defined in AdS, unless boundary conditions are imposed in the surface at $\Psi = \pi/2$. It can be proven that radially directed timelike geodesics starting at the origin will eventually turn around and reconverge at the origin in a finite time $t = \pi$. A more comprehensive review on this subject and the general structure of AdS spacetime can be found in chapter 2 of [42].

Another useful form of the AdS metric is in terms of the usual coordinates (r, t, θ, ϕ):

$$ds^2 = -\left(1 + r^2/L^2\right) dt^2 + \left(1 + r^2/L^2\right)^{-1} dr^2 + r^2 d\Omega^2 \tag{A.15}$$

B. Equations for the Predictor-Corrector method

In section 4.1.2, equation 4.11 introduced an implicit relation for the Y variables. In the following we explicitly write the equation for each one of them. We use the same notation as section 4.1.2 for the points in the grid labelled as m and w:

$$a(m) = \frac{a(w) + \frac{1}{2}ha(w)d(w)}{1 - \frac{1}{2}hd(m)} \tag{B.1}$$

$$s(m) = s(w) + \frac{1}{2}h\left(q(w) + q(m)\right) \tag{B.2}$$

$$r(m) = r(w) + \frac{1}{2}h\left(g(w) + g(m)\right) \tag{B.3}$$

$$g(m) = \frac{g(w) + \frac{1}{2}h\left(2d(w)g(w) - r(w)q^2(w) - r(m)q^2(m)\right)}{1 - hd(m)} \tag{B.4}$$

$$f(m) = \left(f(w) - \frac{1}{2}h\left(\frac{f(w)g(w) + \frac{1}{4}a^2(w)}{r(w)} + \frac{a^2(m)}{4r(m)}\right)\right) \Big/ \left(1 + \frac{hg(m)}{2r(m)}\right) \tag{B.5}$$

$$p(m) = \left(p(w) - \frac{1}{2}h\left(\frac{f(w)q(w) + g(w)p(w)}{r(w)} + \frac{f(m)q(m)}{r(m)}\right)\right) \Big/ \left(1 + \frac{hg(m)}{2r(m)}\right) \tag{B.6}$$

C. Control equations M12 and A12

In order to check the accuracy of our method, we decided to monitor equations M12 and A12. These equations were not used in the integration scheme, but are used to test that our code is working properly. Due to the finite size of the grid, we expect that M12 and A12 will not vanish exactly, but they should remain close to zero.

Figure C.1 shows a plot of M12 as a function of u for a fixed value of $v = 7.5$. The black line is subcritical data (same as figure 5.1), which is dispersed to infinity. The red line is supercritical data which shows three oscillations (same as figure 5.7). In both cases, the control equation M12 remains close to zero, but for the supercritical solution it diverges when it approaches the singularity. The oscillations observed in both cases are due to the profile of the perturbation. In the supercritical case, we used data close to the critical solution, which is reflected by the presence of the three peaks in the solution in red.

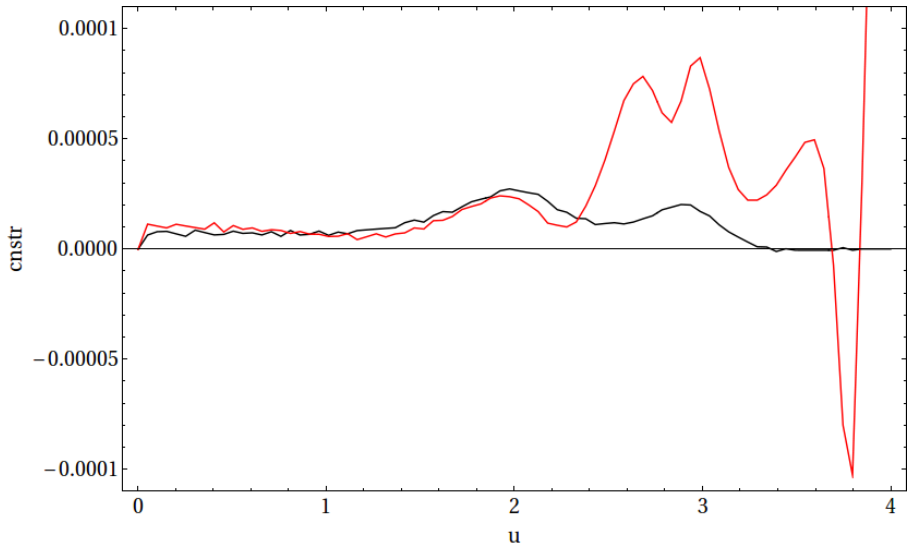

Figure C.1.: Plot of the constraint equation M12 for a subcritical solution (black) and a supercritical solution (red).

In figure C.2 we show a plot of the control equation A12 as a function of u with a

fixed value of $v = 7.5$ for the case $L = 4$. Just as the asymptotically flat case, we show the results for a subcritical solution and a slightly supercritical solution. The control equation remains cloze to zero for the subcritical case and we observe that it diverges when it the solution approaches the singularity in the supercritical case.

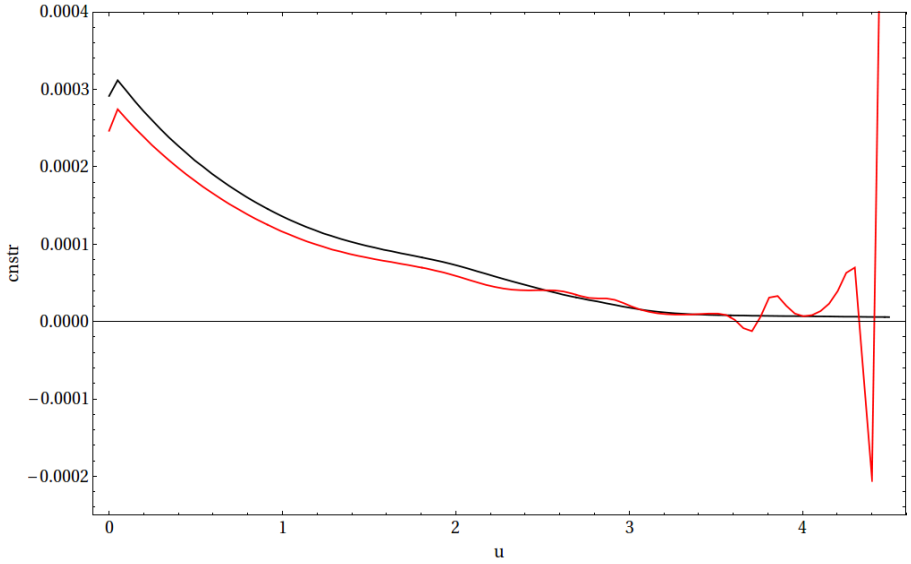

Figure C.2.: Plot of the constraint equation A12 ($L = 4$) for a subcritical solution (black) and a supercritical solution (red).

D. Source code for the simulations in asymptotically flat spacetime

The following is the C source code used for the simulations in asymptotically flat spacetime.

```
#include "stdio.h"
#include "stdlib.h"
#include "math.h"
#include <time.h>

#define SGRID 4000
#define STEP 0.0025
#define PLOTPOINTS 200

double a[SGRID][SGRID],s[SGRID][SGRID],q[SGRID][SGRID],d[SGRID][SGRID],r[SGRID][SGRID],f[SGRID][SGRID],g[SGRID][SGRI

//Functions
void integrate_layer(int), evolint(int);

int main (int argc, const char * argv[]){

//Initial conditions for q and d
double cen,amp,wid,cstep;
cen=2;
amp=0.040240820290225263975412;
wid=2;
int c;
for(c=0;c<SGRID;c++){
cstep=c*STEP;
d[0][c]=0;
q[0][c]=-2*wid*amp*cstep*cstep*(cstep-cen)*exp(-wid*(cstep-cen)*(cstep-cen))+2*amp*cstep*exp(-wid*(cstep-cen)*(cstep
        }
//r value in the boundary
double rb=0.00025;

//boundary conditions at the axis u=v
a[0][0]=1;
r[0][0]=rb;
g[0][0]=0.5*(a[0][0]);
f[0][0]=-g[0][0];
p[0][0]=q[0][0];
s[0][0]=0;

int layer,lc;
integrate_layer(0);

for(layer=1;layer<SGRID;layer++){

//Boundary conditions
for(lc=0;lc<layer;lc++){
a[layer][lc]=0;
s[layer][lc]=0;
r[layer][lc]=0;
g[layer][lc]=0;
f[layer][lc]=0;
```

```
51  d[layer][lc]=0;
52  p[layer][lc]=0;
53  q[layer][lc]=0;
54                  }
55  if(layer==1){
56  a[layer][layer]=a[layer-1][layer+1];
57  s[layer][layer]=s[layer-1][layer+1];
58  }
59  else{
60  a[layer][layer]=(4*a[layer-1][layer+1] - a[layer-2][layer+2])/3;
61  s[layer][layer]=(4*s[layer-1][layer+1] - s[layer-2][layer+2])/3;
62          }
63  r[layer][layer]=rb;
64  g[layer][layer]=0.5*(a[layer][layer]);
65  f[layer][layer]=-g[layer][layer];
66  d[layer][layer]=d[layer-1][layer];
67  q[layer][layer]=q[layer-1][layer];
68  p[layer][layer]=q[layer][layer];
69
70  //Calculate the variables in the next layer
71  evolint(layer);
72          }
73  return 0;
74  }
75
76  //Functions
77  void integrate_layer(int layer){
78
79  int st;
80  double k1, k2, k3, k4, tv;
81
82  for(st=layer;st<SGRID-1;st++){
83
84  //Integrate a
85  k1=STEP*(a[layer][st])*(d[layer][st]);
86  k2=STEP*(a[layer][st]+k1/2)*0.5*(d[layer][st]+d[layer][st+1]);
87  k3=STEP*(a[layer][st]+k2/2)*0.5*(d[layer][st]+d[layer][st+1]);
88  k4=STEP*(a[layer][st]+k3)*(d[layer][st+1]);
89  a[layer][st+1]=a[layer][st]+k1/6+k2/3+k3/3+k4/6;
90
91  //Integrate r
92  k1=STEP*g[layer][st];
93  tv=g[layer][st]+STEP*(2*(d[layer][st])*g[layer][st]-r[layer][st]*q[layer][st]*q[layer][st]);
94  k2=STEP*0.5*(g[layer][st]+tv);
95  k3=k2;
96  k4=STEP*tv;
97  r[layer][st+1]=r[layer][st]+k1/6+k2/3+k3/3+k4/6;
98
99  //Integrate g
100 k1=STEP*(2*(d[layer][st])*g[layer][st]-r[layer][st]*q[layer][st]*q[layer][st]);
101 k2=STEP*(2*(0.5*(d[layer][st]+d[layer][st+1]))*(g[layer][st]+k1/2)-(0.5*(r[layer][st]+r[layer][st+1])*0.5*(q[layer][
102 k3=STEP*(2*(0.5*(d[layer][st]+d[layer][st+1]))*(g[layer][st]+k2/2)-(0.5*(r[layer][st]+r[layer][st+1])*0.5*(q[layer][
103 k4=STEP*(2*(d[layer][st+1])*(g[layer][st]+k3)-(r[layer][st+1])*(q[layer][st+1])*(q[layer][st+1]));
104 g[layer][st+1]=g[layer][st]+k1/6+k2/3+k3/3+k4/6;
105
106 //Integrate s
107 k1=STEP*q[layer][st];
108 k2=STEP*0.5*(q[layer][st]+q[layer][st+1]);
109 k3=k2;
110 k4=STEP*(q[layer][st+1]);
111 s[layer][st+1]=s[layer][st]+k1/6+k2/3+k3/3+k4/6;
112
113 //Integrate f
114 k1=-STEP*(g[layer][st]*(f[layer][st])+0.25*(a[layer][st])*(a[layer][st]))/((r[layer][st]));
115 k2=-STEP*(0.5*(g[layer][st]+g[layer][st+1])*(f[layer][st]+k1/2)+0.25*0.25*(a[layer][st]+a[layer][st+1])*(a[layer][st
116 k3=-STEP*(0.5*(g[layer][st]+g[layer][st+1])*(f[layer][st]+k2/2)+0.25*0.25*(a[layer][st]+a[layer][st+1])*(a[layer][st
117 k4=-STEP*(g[layer][st+1]*(f[layer][st]+k3)+0.25*(a[layer][st+1])*(a[layer][st+1]))/(r[layer][st+1]);
118 f[layer][st+1]=f[layer][st]+k1/6+k2/3+k3/3+k4/6;
119
120 //Integrate p
121 k1=-STEP*(q[layer][st]*(f[layer][st])+(g[layer][st])*(p[layer][st]))/((r[layer][st]));
122 k2=-STEP*(0.5*(g[layer][st]+g[layer][st+1])*(p[layer][st]+k1/2)+0.25*(f[layer][st]+f[layer][st+1])*(q[layer][st]+q[l
```

```
123  k3=-STEP*(0.5*(g[layer][st]+g[layer][st+1])*(p[layer][st]+k2/2)+0.25*(f[layer][st]+f[layer][st+1])*(q[layer][st]+q[l
124  k4=-STEP*(q[layer][st+1]*(f[layer][st+1])+(g[layer][st+1])*(p[layer][st]+k3))/((r[layer][st+1]));
125  p[layer][st+1]=p[layer][st]+k1/6+k2/3+k3/3+k4/6;
126          }
127  }
128
129  void evolint(int layer){
130
131  double aq,ad,bf,bg,bg2,br,bp,bs,c,tq,ba,bq,k1,k2,k3,k4,tv;
132  int sc;
133  for(sc=layer+1;sc<SGRID-1;sc++){
134
135  aq=q[layer-1][sc]-STEP*(f[layer-1][sc]*q[layer-1][sc]+g[layer-1][sc]*p[layer-1][sc])/r[layer-1][sc];
136  ad=d[layer-1][sc]+STEP*((f[layer-1][sc]*g[layer-1][sc]+0.25*a[layer-1][sc]*a[layer-1][sc])/(r[layer-1][sc]*r[layer-
137  bg2=g[layer][sc-1]+STEP*(2*d[layer][sc-1]*g[layer][sc-1]-r[layer][sc-1]*q[layer][sc-1]*q[layer][sc-1]);
138  ba=(a[layer][sc-1] + 0.5*STEP*a[layer][sc-1]*d[layer][sc-1])/(1-0.5*STEP*ad);
139  br=r[layer][sc-1]+0.5*STEP*(g[layer][sc-1]+bg2);
140  bg=(g[layer][sc-1]+0.5*STEP*(2*d[layer][sc-1]*g[layer][sc-1]-r[layer][sc-1]*q[layer][sc-1]*q[layer][sc-1]-br*aq*aq))
141  bf=(f[layer][sc-1]-0.5*STEP*((f[layer][sc-1]*g[layer][sc-1]+0.25*a[layer][sc-1]*a[layer][sc-1])/(r[layer][sc-1]) + 0
142  bp=(p[layer][sc-1]-0.5*STEP*((f[layer][sc-1]*q[layer][sc-1]+g[layer][sc-1]*p[layer][sc-1])/(r[layer][sc-1])+bf*aq/br
143
144  //Evolve q
145  q[layer][sc]=0.5*(aq+q[layer-1][sc]-STEP*(bf*aq+bg*bp)/br);
146
147  //Evolve d
148  d[layer][sc]=0.5*(ad+d[layer-1][sc]+STEP*((bf*bg+0.25*ba*ba)/(br*br)-bp*aq));
149
150  //Integrate the rest of variables
151  //Integrate a
152  k1=STEP*(a[layer][sc-1])*(d[layer][sc-1]);
153  k2=STEP*(a[layer][sc-1]+k1/2)*0.5*(d[layer][sc-1]+d[layer][sc]);
154  k3=STEP*(a[layer][sc-1]+k2/2)*0.5*(d[layer][sc-1]+d[layer][sc]);
155  k4=STEP*(a[layer][sc-1]+k3)*(d[layer][sc]);
156  a[layer][sc]=a[layer][sc-1]+k1/6+k2/3+k3/3+k4/6;
157
158  //Integrate r
159  k1=STEP*g[layer][sc-1];
160  tv=g[layer][sc-1]+STEP*(2*(d[layer][sc-1])*g[layer][sc-1]-r[layer][sc-1]*q[layer][sc-1]*q[layer][sc-1]);
161  k2=STEP*0.5*(g[layer][sc-1]+tv);
162  k3=k2;
163  k4=STEP*tv;
164  r[layer][sc]=r[layer][sc-1]+k1/6+k2/3+k3/3+k4/6;
165
166  //Integrate g
167  k1=STEP*(2*(d[layer][sc-1])*g[layer][sc-1]-r[layer][sc-1]*q[layer][sc-1]*q[layer][sc-1]);
168  k2=STEP*(2*(0.5*(d[layer][sc-1]+d[layer][sc]))*(g[layer][sc-1]+k1/2)-(0.5*(r[layer][sc-1]+r[layer][sc])*0.5*(q[layer
169  k3=STEP*(2*(0.5*(d[layer][sc-1]+d[layer][sc]))*(g[layer][sc-1]+k2/2)-(0.5*(r[layer][sc-1]+r[layer][sc])*0.5*(q[layer
170  k4=STEP*(2*(d[layer][sc])*(g[layer][sc-1]+k3)-r[layer][sc]*q[layer][sc]*q[layer][sc]);
171  g[layer][sc]=g[layer][sc-1]+k1/6+k2/3+k3/3+k4/6;
172
173  //Integrate s
174  k1=STEP*q[layer][sc-1];
175  k2=STEP*0.5*(q[layer][sc-1]+q[layer][sc]);
176  k3=k2;
177  k4=STEP*q[layer][sc-1];
178  s[layer][sc]=s[layer][sc-1]+k1/6+k2/3+k3/3+k4/6;
179
180  //Integrate f
181  k1=-STEP*(g[layer][sc-1]*(f[layer][sc-1])+0.25*(a[layer][sc-1])*(a[layer][sc-1]))/((r[layer][sc-1]));
182  k2=-STEP*(0.5*(g[layer][sc-1]+g[layer][sc])*(f[layer][sc-1]+k1/2)+0.25*0.25*(a[layer][sc-1]+a[layer][sc])*(a[layer][
183  k3=-STEP*(0.5*(g[layer][sc-1]+g[layer][sc])*(f[layer][sc-1]+k2/2)+0.25*0.25*(a[layer][sc-1]+a[layer][sc])*(a[layer][
184  k4=-STEP*(g[layer][sc]*(f[layer][sc-1]+k3)+0.25*(a[layer][sc])*(a[layer][sc]))/((r[layer][sc]));
185  f[layer][sc]=f[layer][sc-1]+k1/6+k2/3+k3/3+k4/6;
186
187  //Integrate p
188  k1=-STEP*(q[layer][sc-1]*(f[layer][sc-1])+(g[layer][sc-1])*(p[layer][sc-1]))/((r[layer][sc-1]));
189  k2=-STEP*(0.5*(g[layer][sc-1]+g[layer][sc])*(p[layer][sc-1]+k1/2)+0.25*(f[layer][sc-1]+f[layer][sc])*(q[layer][sc-1]
190  k3=-STEP*(0.5*(g[layer][sc-1]+g[layer][sc])*(p[layer][sc-1]+k2/2)+0.25*(f[layer][sc-1]+f[layer][sc])*(q[layer][sc-1]
191  k4=-STEP*(q[layer][sc]*(f[layer][sc])+(g[layer][sc])*(p[layer][sc-1]+k3))/((r[layer][sc]));
192  p[layer][sc]=p[layer][sc-1]+k1/6+k2/3+k3/3+k4/6;
193  }
194  }
```

E. Source code for the simulations asymptotically AdS spacetime

The following is the C source code used for the simulations in asymptotically AdS spacetime.

```
#include "stdio.h"
#include "stdlib.h"
#include "math.h"
#include <time.h>

#define SGRID 4000
#define STEP 0.0025
#define PLOTPOINTS 200
#define L2 16

double a[SGRID][SGRID],s[SGRID][SGRID],q[SGRID][SGRID],d[SGRID][SGRID],r[SGRID][SGRID],f[SGRID][SGRID],g[SGRID][SGRI

//Functions
void integrate_layer(int), evolint(int);

int main (int argc, const char * argv[]){

//Initial conditions for q and d
double amp,cen,wid,cstep;
amp=0.05010408899628711314 9758;
wid=2;
cen=2
int c;
for(c=0;c<SGRID;c++){
cstep=c*STEP;
d[0][c]=0.5*tan(cstep/(2*sqrt(L2)))/sqrt(L2);
q[0][c]=-2*wid*amp*cstep*cstep*(cstep-cen)*exp(-wid*(cstep-cen)*(cstep-cen))+2*amp*cstep*exp(-wid*(cstep-cen)*(cstep
        }
//r value in the boundary
double rb=0.00025;

//boundary conditions at the axis u=v
a[0][0]=1;
r[0][0]=rb;
g[0][0]=0.5*(a[0][0]);
f[0][0]=-g[0][0];
p[0][0]=q[0][0];
s[0][0]=0;

int layer,lc;
integrate_layer(0);

for(layer=1;layer<SGRID;layer++){

//Boundary conditions
for(lc=0;lc<layer;lc++){
a[layer][lc]=0;
s[layer][lc]=0;
r[layer][lc]=0;
g[layer][lc]=0;
```

```
51  f[layer][lc]=0;
52  d[layer][lc]=0;
53  p[layer][lc]=0;
54  q[layer][lc]=0;
55                      }
56  if(layer==1){
57  a[layer][layer]=a[layer-1][layer+1];
58  s[layer][layer]=s[layer-1][layer+1];}
59  else{
60  a[layer][layer]=(4*a[layer-1][layer+1] - a[layer-2][layer+2])/3;
61  s[layer][layer]=(4*s[layer-1][layer+1] - s[layer-2][layer+2])/3;
62           }
63  r[layer][layer]=rb;
64  g[layer][layer]=0.5*(a[layer][layer]);
65  f[layer][layer]=-g[layer][layer];
66  d[layer][layer]=d[layer-1][layer];
67  q[layer][layer]=q[layer-1][layer];
68  p[layer][layer]=q[layer][layer];
69
70  //Calculate the variables in the next layer
71  evolint(layer);
72  }
73  return 0;
74  }
75
76  void integrate_layer(int layer){
77
78  int st;
79  double k1, k2, k3, k4, tv;
80
81  for(st=layer;st<SGRID-1;st++){
82
83  //Integrate a
84  k1=STEP*(a[layer][st])*(d[layer][st]);
85  k2=STEP*(a[layer][st]+k1/2)*0.5*(d[layer][st]+d[layer][st+1]);
86  k3=STEP*(a[layer][st]+k2/2)*0.5*(d[layer][st]+d[layer][st+1]);
87  k4=STEP*(a[layer][st]+k3)*(d[layer][st+1]);
88  a[layer][st+1]=a[layer][st]+k1/6+k2/3+k3/3+k4/6;
89
90  //Integrate r
91  k1=STEP*g[layer][st];
92  tv=g[layer][st]+STEP*(2*(d[layer][st])*g[layer][st]-r[layer][st]*q[layer][st]*q[layer][st]);
93  k2=STEP*0.5*(g[layer][st]+tv);
94  k3=k2;
95  k4=STEP*tv;
96  r[layer][st+1]=r[layer][st]+k1/6+k2/3+k3/3+k4/6;
97
98  //Integrate g
99  k1=STEP*(2*(d[layer][st])*g[layer][st]-r[layer][st]*q[layer][st]*q[layer][st]);
100 k2=STEP*(2*(0.5*(d[layer][st]+d[layer][st+1]))*(g[layer][st]+k1/2)-(0.5*(r[layer][st]+r[layer][st+1])*0.5*(q[layer][
101 k3=STEP*(2*(0.5*(d[layer][st]+d[layer][st+1]))*(g[layer][st]+k2/2)-(0.5*(r[layer][st]+r[layer][st+1])*0.5*(q[layer][
102 k4=STEP*(2*(d[layer][st+1])*(g[layer][st]+k3)-(r[layer][st+1])*(q[layer][st+1])*(q[layer][st+1]));
103 g[layer][st+1]=g[layer][st]+k1/6+k2/3+k3/3+k4/6;
104
105 //Integrate s
106 k1=STEP*q[layer][st];
107 k2=STEP*0.5*(q[layer][st]+q[layer][st+1]);
108 k3=k2;
109 k4=STEP*(q[layer][st+1]);
110 s[layer][st+1]=s[layer][st]+k1/6+k2/3+k3/3+k4/6;
111
112 //Integrate f
113 k1=-STEP*(g[layer][st]*(f[layer][st])+0.25*(a[layer][st])*(a[layer][st]))/((r[layer][st]))-0.75*STEP*(r[layer][st]*a
114 k2=-STEP*(0.5*(g[layer][st]+g[layer][st+1])*(f[layer][st]+k1/2)+0.25*0.25*(a[layer][st]+a[layer][st+1])*(a[layer][st
115 k3=-STEP*(0.5*(g[layer][st]+g[layer][st+1])*(f[layer][st]+k2/2)+0.25*0.25*(a[layer][st]+a[layer][st+1])*(a[layer][st
116 k4=-STEP*(g[layer][st+1]*(f[layer][st]+k3)+0.25*(a[layer][st+1])*(a[layer][st+1]))/((r[layer][st+1]))-0.75*STEP*(r[l
117 f[layer][st+1]=f[layer][st]+k2;
118
119 //Integrate p
120 k1=-STEP*(q[layer][st]*(f[layer][st])+(g[layer][st])*(p[layer][st]))/((r[layer][st]));
121 k2=-STEP*(0.5*(g[layer][st]+g[layer][st+1])*(p[layer][st]+k1/2)+0.25*(f[layer][st]+f[layer][st+1])*(q[layer][st]+q[l
122 k3=-STEP*(0.5*(g[layer][st]+g[layer][st+1])*(p[layer][st]+k2/2)+0.25*(f[layer][st]+f[layer][st+1])*(q[layer][st]+q[l
```

```
k4=-STEP*(q[layer][st+1]*(f[layer][st+1])+(g[layer][st+1])*(p[layer][st]+k3))/((r[layer][st+1]));
p[layer][st+1]=p[layer][st]+k1/6+k2/3+k3/3+k4/6;
}
}

void evolint(int layer){

double aq,ad,bf,bg,br,bp,c,tq,ba,bq,bg2,k1,k2,k3,k4,tv;
int sc;
for(sc=layer+1;sc<SGRID-1;sc++){

aq=q[layer-1][sc]-STEP*(f[layer-1][sc]*q[layer-1][sc]+g[layer-1][sc]*p[layer-1][sc])/r[layer-1][sc];
ad=d[layer-1][sc]+STEP*((f[layer-1][sc]*g[layer-1][sc]+0.25*a[layer-1][sc]*a[layer-1][sc])/(r[layer-1][sc]*r[layer-
bg2=g[layer][sc-1]+STEP*(2*d[layer][sc-1]*g[layer][sc-1]-r[layer][sc-1]*q[layer][sc-1]*q[layer][sc-1]);
ba=(a[layer][sc-1] + 0.5*STEP*a[layer][sc-1]*d[layer][sc-1])/(1-0.5*STEP*ad);
br=r[layer][sc-1]+0.5*STEP*(g[layer][sc-1]+bg2);
bg=(g[layer][sc-1]+0.5*STEP*(2*d[layer][sc-1]*g[layer][sc-1]-r[layer][sc-1]*q[layer][sc-1]*q[layer][sc-1]-br*aq*aq))
bf=(f[layer][sc-1]-0.5*STEP*((f[layer][sc-1]*g[layer][sc-1]+0.25*a[layer][sc-1]*a[layer][sc-1])/(r[layer][sc-1]) + 0
bp=(p[layer][sc-1]-0.5*STEP*((f[layer][sc-1]*q[layer][sc-1]+g[layer][sc-1]*p[layer][sc-1])/(r[layer][sc-1])+bf*aq/br

//Evolve q
q[layer][sc]=0.5*(aq+q[layer-1][sc]-STEP*(bf*aq+bg*bp)/br);

//Evolve d
d[layer][sc]=0.5*(ad+d[layer-1][sc]+STEP*((bf*bg+0.25*ba*ba)/(br*br)-bp*aq));

//Integrate the rest of variables

//Integrate a
k1=STEP*(a[layer][sc-1])*(d[layer][sc-1]);
k2=STEP*(a[layer][sc-1]+k1/2)*0.5*(d[layer][sc-1]+d[layer][sc]);
k3=STEP*(a[layer][sc-1]+k2/2)*0.5*(d[layer][sc-1]+d[layer][sc]);
k4=STEP*(a[layer][sc-1]+k3)*(d[layer][sc]);
a[layer][sc]=a[layer][sc-1]+k1/6+k2/3+k3/3+k4/6;

//Integrate r
k1=STEP*g[layer][sc-1];
tv=g[layer][sc-1]+STEP*(2*(d[layer][sc-1])*g[layer][sc-1]-r[layer][sc-1]*q[layer][sc-1]*q[layer][sc-1]);
k2=STEP*0.5*(g[layer][sc-1]+tv);
k3=k2;
k4=STEP*tv;
r[layer][sc]=r[layer][sc-1]+k1/6+k2/3+k3/3+k4/6;

//Integrate g
k1=STEP*(2*(d[layer][sc-1])*g[layer][sc-1]-r[layer][sc-1]*q[layer][sc-1]*q[layer][sc-1]);
k2=STEP*(2*(0.5*(d[layer][sc-1]+d[layer][sc]))*(g[layer][sc-1]+k1/2)-(0.5*(r[layer][sc-1]+r[layer][sc])*0.5*(q[layer
k3=STEP*(2*(0.5*(d[layer][sc-1]+d[layer][sc]))*(g[layer][sc-1]+k2/2)-(0.5*(r[layer][sc-1]+r[layer][sc])*0.5*(q[layer
k4=STEP*(2*(d[layer][sc])*(g[layer][sc-1]+k3)-r[layer][sc]*q[layer][sc]*q[layer][sc]);
g[layer][sc]=g[layer][sc-1]+k1/6+k2/3+k3/3+k4/6;

//Integrate s
k1=STEP*q[layer][sc-1];
k2=STEP*0.5*(q[layer][sc-1]+q[layer][sc]);
k3=k2;
k4=STEP*q[layer][sc-1];
s[layer][sc]=s[layer][sc-1]+k1/6+k2/3+k3/3+k4/6;

//Integrate f
k1=-STEP*(g[layer][sc-1]*(f[layer][sc-1])+0.25*(a[layer][sc-1])*(a[layer][sc-1]))/((r[layer][sc-1]))-0.75*STEP*(r[la
k2=-STEP*(0.5*(g[layer][sc-1]+g[layer][sc])*(f[layer][sc-1]+k1/2)+0.25*0.25*(a[layer][sc-1]+a[layer][sc])*(a[layer][
k3=-STEP*(0.5*(g[layer][sc-1]+g[layer][sc])*(f[layer][sc-1]+k2/2)+0.25*0.25*(a[layer][sc-1]+a[layer][sc])*(a[layer][
k4=-STEP*(g[layer][sc]*(f[layer][sc]+k3)+0.25*(a[layer][sc])*(a[layer][sc]))/((r[layer][sc]))-0.75*STEP*(r[layer][sc
f[layer][sc]=f[layer][sc-1]+k1/6+k2/3+k3/3+k4/6;

//Integrate p
k1=-STEP*(q[layer][sc-1]*(f[layer][sc-1])+(g[layer][sc-1])*(p[layer][sc-1]))/((r[layer][sc-1]));
k2=-STEP*(0.5*(g[layer][sc-1]+g[layer][sc])*(p[layer][sc-1]+k1/2)+0.25*(f[layer][sc-1]+f[layer][sc])*(q[layer][sc-1]
k3=-STEP*(0.5*(g[layer][sc-1]+g[layer][sc])*(p[layer][sc-1]+k2/2)+0.25*(f[layer][sc-1]+f[layer][sc])*(q[layer][sc-1]
k4=-STEP*(q[layer][sc]*(f[layer][sc])+(g[layer][sc])*(p[layer][sc-1]+k3))/((r[layer][sc]));
p[layer][sc]=p[layer][sc-1]+k1/6+k2/3+k3/3+k4/6;
}
}
```